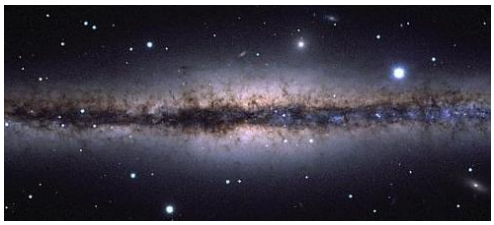

DEPARTMENT OF ASTRONOMY
The University of Wisconsin-Madison
475 N Charter Street
Madison Wisconsin 53706-1582
Telephone: (608) 262-3071
FAX: (608) 263-6386
http://www.astro.wisc.edu

DOCUMENT IDENTIFICATION:

PROJECT:	**SOUTHERN AFRICAN LARGE TELESCOPE** **ROBERT STOBIE SPECTROGRAPH** **NEAR INFRARED INSTRUMENT**
DOCUMENT TITLE:	**SCIENCE DRIVERS**
DOCUMENT #:	**SALT-3501AS0001**
FILENAME:	
REVISION:	-
KEYWORDS:	

APPROVALS:

AUTHOR:	_____ Date:_____ Marsha Wolf Project Scientist
ENGINEERING:	_____ Date:_____ Don Thielman System Engineer
QUALITY:	_____ Date:_____ Tom Demke Quality Assurance
PROJECT:	_____ Date:_____ Andy Sheinis Principal Investigator

REVISION HISTORY:

Rev	ECN	Description	Date	Approval
Draft	NA	Original Document	18 May 2009	

Compiled by Marsha Wolf with assistance from Amy Barger, Matthew Bershady, David Buckley, Ed Chruchwell, Jay Gallagher, Eric Hooper, Anand Narayanan, Kenneth Nordsieck, Andrew Sheinis, Christy Tremonti, Bev Wills

Table of Contents

1 Introduction

Many of the breakthroughs and advances in astrophysics are enabled by advances in instrumentation. New discoveries or understanding always follow the opening of new observational parameter space. Although infrared observations have been conducted for quite some time, particularly for imaging, efficient near infrared (NIR) spectrographs on 10-meter class telescopes with multiplexing capability are only now beginning to come to fruition. With such instruments large surveys of faint high redshift objects can be conducted and hidden objects enshrouded in dust can be studied in detail.

The Robert Stobie Spectrograph Near Infrared Arm (RSS-NIR) will fill this instrumentation gap on the 11-meter Southern African Large Telescope (SALT). To set the science case for RSS-NIR we begin with a general outline of prime research areas for NIR studies in Section 1.1, with specific interests of scientists within the SALT consortium listed in Section 2. Individual researchers on the RSS-NIR science team are presented in Section 3. Instrument specifics are discussed in Section 4, which begins with a brief overview of the RSS-NIR capabilities, discusses constraints imposed on NIR observations (such as the bright night sky), and gives a general description of the anticipated use of each instrument mode with these constraints in mind. RSS-NIR is compared to other NIR instruments on 4-10 meter class instruments worldwide in Section 5, including performance predictions. One of the main science cases from researchers at the University of Wisconsin is presented in Section 6, with overviews of additional projects described in Sections 7-8. The science requirements for RSS-NIR are summarized in Section 11 and we conclude with a science-engineering decision trade matrix for the instrument in Section11.1 and an overview of the resulting baseline system in Section 11.2.

1.1 Research Areas in the NIR

The NIR regime can be used to probe objects that would not otherwise be accessible in optical wavelengths. Hidden objects embedded in obscuring dust can be studied, new NIR spectral features and diagnostics may be observed and defined, and redshifted spectral features that are normally used for galaxy diagnostics in optical bands can be observed in much more distant objects. We outline a few key areas of research below.

Young stars ***(Chruchwell – UW, Vink - Armagh Observatory)*****.** Although star formation rates estimated from light integrated over entire galaxies are routinely used as a cosmological diagnostic for galaxy evolution throughout the universe, the details of actual star formation are not very well understood. One problem is that stars form inside molecular clouds that are dense and typically have optical extinctions on the order of 10's of magnitudes. NIR spectrographs can peer though this dust to study details of the young stellar objects and their lingering disks. In order to probe the circumstellar geometry of the most massive young stellar objects, we must use diagnostics at NIR wavelengths, as the more massive young stellar objects remain optically obscured throughout their entire pre-main sequence lives. Multi-object capability is important for studying forming and young star clusters still embedded in molecular clouds. The 8 arcmin field of view of RSS is well matched to their sizes in nearby regions of the Milky Way.

Low mass stars ***(Churchwell – UW)*****.** The stellar initial mass function (IMF) is very important for understanding global star formation and for properly doing stellar population synthesis of galaxies.

Much of what is currently known about star formation is on the high mass end. The low end of the IMF is virtually unknown because these stars are very faint and red. NIR spectrographs on 10-m class telescopes will be able to characterize the low end of the stellar IMF.

Brown dwarfs. Brown dwarfs fall in between stars and planets in mass and atmospheric properties. Studying their formation will help us to understand the bigger picture of the formation of both stars and planets. One interesting aspect is that no brown dwarf companions have been found to low mass stars, while other low mass stars and planets do exist in such pairs. This suggests that there is something we do not understand about the formation of brown dwarf mass objects. Brown dwarfs harbor more complex atmospheres than stars or planets. Their spectra peak in the NIR and contain a number of molecular band and atomic absorption features. Weather causes variability, so wide simultaneous spectral coverage at a resolution of $R \geq 5000$ will be important in their study. Their low intrinsic luminosities necessitate instruments on large telescopes.

Cool stars ***(Gallagher – UW).*** Red supergiants and red giants are the most luminous stars in, respectively, star forming or old passive galaxies. In highly reddened starburst galaxies, the NIR light from red supergiants is sometimes the only direct information available on the stellar populations. Models for their spectra are thus important, even though they are also particularly difficult to construct due to their rich molecular line spectra and extended atmospheres. However, if the models are successful in reproducing empirical spectra, they can be used instead of observed spectral libraries in future analyses of galaxies. At NIR wavelengths (1–2.5 μm), the most prominent molecular features in these stars are those of CO and CN, which have sensitivity to surface gravity and effective temperature (Lancon et al. 2007). Adding to the library of observed spectra of these stars will help to improve stellar population synthesis models.

Multi-component systems. RSS-NIR will be a powerful instrument for observing phase-resolved systems such as compact binaries. The visible and NIR spectral regions can be used to observe the two different components in the system. Simultaneous observations are necessary because these systems are known to be time-variable.

Supernova explosion physics ***(Nordsieck – UW).*** One important aspect of supernovae (SNe) that is not yet well understood is their asymmetry, which may impact their observed brightness (in the case of SNe Ia) as well as the deposition of kinetic energy and enriched material into their environment. Observational probes of SN asymmetries have been challenging: the most effective way of probing the asymmetries in SNe is with spectropolarimetry, and this has been pursued only recently with the advent of spectropolarimeters on 10-meter class telescopes. In SNe, a net continuum polarization of the integrated light results from an asymmetry of the photosphere, while polarization in the P-Cygni lines results from asymmetries in the overlying ejecta. By measuring the variation of line polarization with wavelength, we can observe asymmetries as a function of velocity (in SNe, this is equivalent to radius) so that line polarization gives us information about chemical and density inhomogeneities within the ejecta, which can then be compared with the results of explosion codes. Different lines show different polarization, indicating that the thermonuclear processing of the explosion is inhomogeneous. RSS-NIR will be the first instrument capable of SNe spectropolarimetry in the NIR on a large telescope, bringing in

a range of unobserved lines that are important for constraining explosion physics models. Especially interesting in SN Ia are the Mg II lines at 1.15 and 1.55 μm. Combining information from these lines with those of Si and Ca, simultaneously observed in the visible, will trace elements produced in the full range of the thermonuclear explosion chain for the first time. Following each SN regularly throughout its light curve will show how this evolves as the envelope becomes optically thin. SALT's queue scheduling readily enables such target of opportunity and synoptic observations. A statistical study of a number of SNe will then determine whether SNe can be divided into further subclasses based on structure (see Section 7).

Gamma ray bursts ***(Buckley – SAAO).*** In gamma ray bursts (GRBs) wide spectral coverage is needed to identify the type of object and its redshfit. Rapid time-evolution of the spectrum and fading generally does not allow the luxury of observing sequentially with visible and NIR instruments with long time delays in between. The queue scheduling and target-of-opportunity nature of SALT makes it a good instrument for catching GRBs soon after discovery when they are bright before the rapid fading of their afterglows. Their unpredictable redshift is a strong reason for making the wavelength coverage as wide as possible. Observations into the NIR would allow identification out to redshifts of $z \geq 10$. RSS-NIR has the unique capability of also doing NIR spectropolarimetry of these objects with an 11 meter telescope.

Stellar populations in nearby starburst galaxies ***(Gallagher – UW).*** Starburst galaxies host large numbers of star clusters. NIR spectroscopy breaks a strong degeneracy between age and extinction in the NIR colors of the red supergiant-dominated phase of stellar evolution in these clusters. The use of extended spectra allows the constraint of both the ages and the shape of the extinction law near inhomogeneously dusty massive star clusters. IR-bright star clusters in M82 have been found to be the product of recent episodes of star formation in the galaxy (Gallagher et al. 2008). Although NIR derived ages from these spectra sometimes disagree with optically derived ages because they sample different populations, they add important elements to the age distribution of massive clusters in dusty starbursts. Joint optical and NIR spectroscopic studies will provide strong constraints on the uncertain physics of massive stars on which the accuracy of population synthesis models rest.

Interaction-triggered starbursts ***(Gallagher – UW).*** There are spectral features in the λ = 1.45 - 1.67 μm NIR wavelength region that are indicative of thermal shocks from supernova remnants ([Fe II] at 1.644 μm) and recombination processes in young HII regions (Br 12-4 at 1.641 μm, Br 13-4 at 1.611 μm, and Br 14-4 at 1.588 μm). By determining the spatial distributions of these emission lines and using the timescales associated with each process, past interaction-induced star formation episodes in nearby galaxies can be deduced (de Grijs et al. 2004). Adding to this information the ages, masses, and spatial distribution of young massive star clusters will tell quite detailed histories of past interactions and star formation episodes in nearby galaxies.

Surveys of galaxies at z > 1 ***(Gawiser – Rutgers, Bershady, Wolf – UW, Kannappan - UNC).*** Spectral features typically used to date stellar populations in passively evolving red galaxies are shifted out of the optical band at $z > 1$. Referring to **Figure 1**, at $z = 1.5$ absorption features used to characterize early-type galaxies, the 4000 Å break, Mg I (5183 Å), Hα, Hβ, and Hγ, , will all be shifted into the NIR bandpass. In

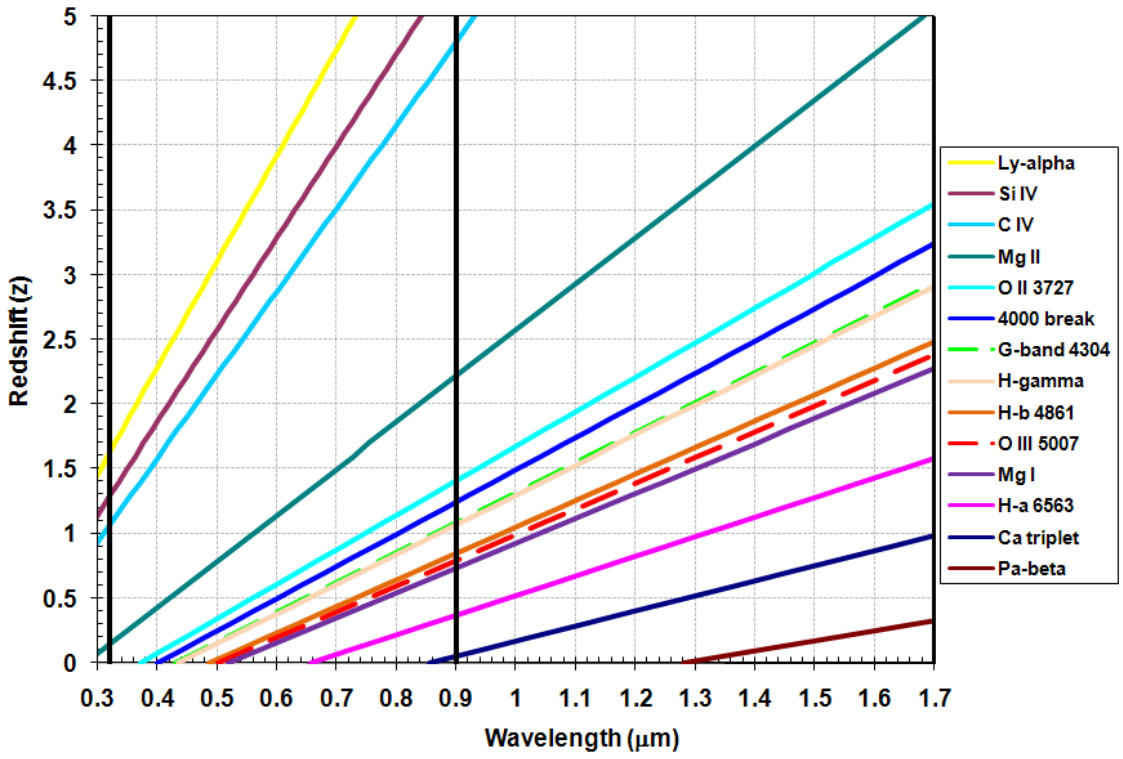

Figure 1. Redshifted spectral features.

galaxies containing dust, the reddening can be estimated from the Hα/Hβ Balmer decrement at z ~ 0.5 using simultaneous RSS-vis and RSS-NIR spectra, and at z > 1 using just RSS-NIR.

Disentangling age and metallicity in galaxies ***(Wolf – UW).*** Much progress has been made in estimating the ages of galaxies by fitting continually improving stellar population synthesis models to their spectra. However, even when the entire optical spectrum of a galaxy is used the age-metallicity degeneracy is still prevalent in model fits to the data. This is particularly true for low S/N spectra typical of individual galaxies in large surveys, in which line indices for determining metallicity are unreliable due to the noisy data. Often the metallicity has to be assumed to determine an age or a number of discrete ages of the stellar populations in a galaxy. Nevertheless, this is one case where wide spectral coverage does help. It has been shown that extending the galaxy spectrum into the NIR helps to disentangle this degeneracy (Wolf 2005). When age and metallicity are both estimated from fits to optical galaxy spectra with S/N $\leq$ 10, the lowest metallicities included in the model grid are often chosen as the best fit by minimizing χ^2, since the low metallicity model spectra tend to have smaller absorption lines. However, when NIR spectra are added to the fit, more realistic estimates of metallicity result. UV-vis-NIR galaxy surveys will provide spectra that should allow reliable analyses of individual galaxies in the surveys.

Galaxy evolution ***(Wolf, Sheinis, Hooper, Tremonti – UW).*** Galaxy mergers play an important role in the growth and evolution of galaxies. Many host galaxies of AGN show signs of past mergers, suggesting that the AGN may be triggered during a phase of the merger. The host galaxies of quasars, systems in

which the supermassive black holes are actively feeding, with high masses show properties similar to giant elliptical galaxies, have obvious signs of past interaction with disturbed morphologies (Wolf & Sheinis 2008), and may be the products of "dry" mergers of two massive progenitor galaxies. These objects tend to be radio-loud. The quasar hosts with intermediate masses show properties similar to quiescent merger remnant galaxies and ultraluminous IR galaxies (ULIRGs), suggesting that they may have formed through gas-rich galaxy mergers that caused a nuclear starburst (Dasyra et al. 2007). These objects tend to be radio-quiet. E+A galaxies are post-starburst galaxies that contain a significant stellar population with an age of approximately 1 Gyr, probably formed during a merger that happened that long ago, as often evidenced by morphological signs of past interactions. Many have been shown to be liners (Yang et al. 2006) or contain optically obscured AGN seen as variable radio point sources (Hooper et al. 2007). The Fabry-Perot mode of RSS-NIR will provide the ability to study details of these systems by imaging Hα or [O II] on the visible arm to look for spatially distributed star formation, while simultaneously looking for shocks with [Fe II] lines or recombination processes in H II regions with Br lines on the NIR arm. Because the two observations will simultaneously access the same field, the spatial maps will automatically be aligned, easing interpretation of past interactions. Interaction and star formation histories of these systems will be much better understood after such observations.

"First Light" surveys ***(Barger, Bershady – UW).*** The new frontier in extragalactic astronomy and cosmology lies at z > 7, when the universe emerged from a period known as the "cosmic dark age." This epoch is marked by the formation of the first (Pop III) stars in proto-galactic units, i.e., "First Light." The observational approach to finding these objects is challenging because the key diagnostic, Lyα, is shifted beyond 1 μm (the end of the optical window) at z > 7. Adding NIR capability enables searches for Lyα emitters up to z~12. Such searches utilizing a NIR Fabry-Perot system, with simultaneous visible Fabry-Perot observations to eliminate interlopers will be very powerful. This is an important science program planned for RSS-NIR by UW researchers (see Section 6.1).

NIR diagnostics of active galactic nuclei ***(Hooper – UW, Wills – UT)***. The near-infrared range covered by RSS-NIR is home to several permitted emission lines of H and He with fluxes ~ few percent to 10% of that of H-alpha; e.g., Paβ at λ = 1.28 μm and He I at λ = 1.08 μm (Glickman, Helfand, & White 2006). These are accessible by RSS-NIR to modest redshifts (z = 0.25 for Paβ, z = 0.48 for He I). Simultaneous access to Paschen and Balmer lines allows a robust determination of extinction to the time variable broad line region (BLR) near the heart of the active galactic nucleus (AGN) central engine, since pairs of Paschen and Balmer lines share a common upper principle quantum level, e.g., Hγ/Paβ, Hδ/Paγ, etc (Paα is beyond the long-wavelength cutoff of RSS-NIR). While heavily obscured central engines will remain hidden, the light gathering power of SALT will enable application of this technique from low to moderate extinctions, such as sight lines that pierce the edges of the AGN dust torus or even occasionally pass through the main part of the torus if it is clumpy (Nenkova et al. 2008).

Several forbidden coronal lines are also present in the part of the spectrum accessible to RSS-NIR, including [S VIII] at λ = 0.99 μm, [Fe XIII] at λ = 1.07 μm, [S IX] at λ = 1.25 μm, and [Si X] at λ = 1.43 μm. While these are typically fainter than the prominent near-IR permitted lines, they have been detected in many nearby active galaxies with 3-4-meter class telescopes (Ramos Almeida, Perez Garcia, & Acosta-

Pulido 2009; Portilla, Rodriguez-Ardila, & Tejeiro 2008), indicating their potential broad utility with an 11-meter telescope. These coronal lines come from species with such large ionization potentials (100 to several hundred eV) that they are unambiguous indicators of the presence of AGN and sample the hard ionizing spectrum of the central engine. They may provide an additional means of estimating black hole mass that is robust against the presence of a strong starburst (due to the high ionization potentials), as was recently found using space-based data for mid-infrared lines from [Ne V] and [O IV] (Dasyra et al. 2008).

Reverberation mapping of AGN ***(Hooper – UW, Wils - UT)*****.** Evidence from broad-band reverberation mapping in the optical and NIR suggests that the BLR size is set by the inner edge of the dusty torus, which is itself determined by the point at which the dust reaches the sublimation temperature of the most robust grains (Clavel, Wamsteker, & Glass 1989; Suganuma et al. 2006). Variations in the J band closely track those in the optical, and the longer wavelength bands from H band onward have progressively larger lags with respect to the optical. This is consistent with the hottest dust component, which lies closest to the central engine, contributing to the H band flux. If this scenario is widely true, the dependence of the sublimation radius on luminosity naturally explains the proportionality between BLR radius and (AGN bolometric luminosity)$^{1/2}$ that is routinely employed to estimate black hole masses in active galaxies (Laor 2007). While dedicated multiwavelength AGN monitoring campaigns have compiled impressive databases, many of the observations are broadband photometry (e.g., the MAGNUM project, Suganuma et al. 2006), and the number of objects is small, a fact lamented in light of the variety of multiwavelength variability characteristics seen in AGN (Gaskell 2008). The RSS optical + NIR combination provides the opportunity to spectroscopically reverberation map the broad lines and the hottest dust component simultaneously, thereby probing the size scale and structure of the BLR/dust torus interface. Extending these observations to new AGN of varying type will determine whether the sublimation radius of the dust torus is a common limiting factor for BLR size. Only the hottest dust will be detectable by RSS-NIR (e.g., a 2000 K emitter peaks at λ = 1.45 μm), but that is precisely what we need to detect the inner edge of the torus. SALT's large aperture and queue scheduling will enable rapid observations of bright AGN (H ~ 12 - 15 mag, similar to targets in Suganuma et al. 2006), which can be observed with the lowest resolution grating, providing the widest contiguous spectral coverage, for long-term monitoring of several objects without a very large outlay of observing time. The telescope/instrument combination is also well suited to pushing these techniques to a few fainter AGN, in which case the gratings at R ~ 4000 would be used to sample between the sky lines.

Quasar absorption line studies of high-z galaxies ***(Narayanan – UW)*****.** Quasar absorption line spectroscopy in the near-IR will be an efficient technique for detecting H I gas and associated metals in the disks and extended gaseous halos of high-z galaxies. Since the absorption technique is unbiased by luminosity, the NIR observations would supplement the existing high-z photometric and spectroscopic samples that are biased towards the higher end of the galaxy luminosity function. Among the various classes of quasar absorbers, the strong Mg II systems are often found within close impact parameters (d $\leq$ 75 kpc) of L > 0.1 L* galaxies (Steidel & Sargent 1992). Numerous spectroscopic absorption line surveys in the optical have offered a full census of this absorber population over the redshift interval 0.4 < z < 2.4. At z > 2.4, the MgII doublet lines are redshifted into the NIR (λ > 0.9 μm). The z > 2.4 regime

corresponds to the epoch where galaxies seem to have gone through significant morphological and chemical evolution, as revealed by the large population of Lyman-break galaxies, sub-mm galaxies (Smail et al. 1997) and galaxies with peculiar morphologies or irregular luminosity profiles (Elmegreen et al. 2005). At z ~ 1 Nestor et al. (2007) have detected a number of *very* strong MgII absorbers (rest equivalent width ~ 4 Å) with kinematically broad (Δv ~ 400 km/s) line profiles. Follow-up imaging observations from the ground have shown that these absorption systems are mostly associated with galaxy pairs that are in the process of interacting and merging, thus contributing to the large velocity spreads. Through NIR observations of luminous quasars at z > 3, it will be possible to detect similar absorption systems at higher redshifts (z > 2.4) and thus select galaxy pairs and interacting systems. The NIR sample would allow us to also observationally constrain the redshift number density evolution of such systems.

Quasar absorption line studies of the IGM ***(Narayanan – UW).*** Near-IR spectroscopy of z > 5 quasars can be used to study the distribution of metals associated with the IGM close to the epoch of reionization. Several groups (Ryan-Weber et al. 2006, Becker et al. 2008) have succeeded in detecting CIV doublet absorption lines in the IGM at those early epochs through moderate resolution spectroscopy in the NIR using ISSAC/VLT and NIRSPEC/Keck. Such observations enabled the estimation of the mass density of metals in the IGM. The apparent lack of evolution in the mass density of metals over 1.4 < z < 5.4, corresponding to a significant fraction of the history of the universe, is an unresolved mystery. The results are however limited by a small sample size. Detection of metals at higher-z (z ~ 5.5) over a sufficiently large number of sight lines (~ 50) would set a constraint on the nature of sources (star-forming galaxies vs. pop III stars) that were responsible for the enrichment of IGM with metals at those early epochs and also measure any differential variation that might exist in their distribution.

2 Science Interests of the SALT Consortium

2.1 Highest Redshift Forming Galaxies (z > 7)

- Very high redshift Ly-α emitters (Barger, Bershady, *UW*)

2.2 High Redshift (2.5 < z < 5.5)

- QSO absorption line studies of interacting galaxies and the IGM (Narayanan, Savage, *UW*)

2.3 Moderate Redshift Galaxies (z ~ 0.5-2)

- Redshifted galaxies, AGN, QSO hosts – stars and gas (Sheinis & Wolf, *UW*)
- Very faint high-z galaxies (Gawiser, *Rutgers*)
- Faint galaxies at z > 0.5 (Menanteau, *Rutgers*)
- High z galaxy kinematics (Kannappan, *UNC*)
- Faint z > 1 galaxies (Aragon-Salamanca, *Nottingham – UK*)
- Low/high redshift galaxies, AGN (Kollatschny for exgal group, *Gottingen*)
- Feedback in galaxies from AGN or star formation, galaxy evolution (Tremonti, *UW*)
- Star forming galaxies: SFRs, nebular abundances (Bershady, *UW*)
- Star-forming galaxies, HII regions, planetary nebulae, mergers (Kniazev, *SAAO*)

- Galaxies in clusters, starbursting galaxies (Crawford, *SAAO*)
- Faint galaxies in clusters (Hughes, *Rutgers*)

2.4 Nearby Galaxies (z < 0.5)

- Quasars and host galaxies – stars and gas (Sheinis & Wolf, *UW*)
- Nearby galaxies and their components (Sparke, *UW*; Bershady, *UW*)
- M82 (Gallagher, *UW*)
- Stellar populations in LMC and SMC (Gallagher, *UW*)
- E+A galaxies as a phase in galaxy evolution: obscured AGN, star formation (Wolf, Hooper, *UW*)
- Strongly star-forming galaxies, interacting galaxies, AGN (Vaisanen, *SAAO*)
- Low/high redshift galaxies, AGN (Kollatschny for exgal group, *Gottingen*)
- Galaxy clusters out to z~0.6 (Vaisanen, *SAAO*)
- NIR diagnostics of AGN (Hooper, *UW;* Wills, *HET-UT Austin*)

2.5 The Milky Way

2.5.1 Star formation

- Ioninzed gas and shocks in nearby star forming regions (Churchwell, *UW*)
- Low end of the stellar initial mass function, IMF (Churchwell, *UW*)
- Star formation emission lines (Gallagher, Bershady, *UW*)

2.5.2 Interstellar Medium

- Nebular fluorescence lines (Nordsieck, *UW*)

2.5.3 Stars

- Emission line stars (Shara, *AMNH*)
- Young massive stars (Vink, *Armagh Observatory – UK*)
- Circumstellar regions of young massive stars (Nordsieck, *UW*)
- Cool stars; dust obscured sources; stellar populations in Fornax and the bulge; AGB stars (Gallagher, *UW*)
- LMXRB, (Buckley, *SAAO*; Kaluzny, *CAMK Poland*)
- Binary brown dwarfs (Kaluzny, *CAMK Poland*)
- Magnetic CVs (Potter, Buckley, *SAAO*)

2.5.4 Supernova

- Faint, late-time emission of supernovae (all types) & galactic/extragalactic nebula (Fesen, *Dartmouth*)
- Features in galactic supernova remnants (Hughes, *Rutgers*)

2.6 Solar System

- Asteroids, Kuiper Belt Objects (Gulbis, *SAAO*)

2.7 Miscellaneous

- Exoplanet transits (Buckley, *SAAO*)
- Gamma ray bursts (Buckley, *SAAO*)

3 RSS-NIR Science Team

Scientists within the SALT consortium who have contributed to the RSS-NIR science drivers are listed below.

Alfonso Aragon-Salamanca: *Professor of Astronomy at University of Nottingham – UK*. Main science interests are extragalactic astronomy and observational cosmology, combining detailed studies of local galaxies with observations of the galaxy population at intermediate and high redshifts.

Amy Barger: *Associate Professor of Astronomy at University of Wisconsin – Madison*. Main science interests are observational cosmology; distant galaxies and supermassive black holes; observations at X-ray, optical, near-infrared, submillimeter, and radio wavelengths; and star formation and accretion histories of the universe.

Matthew Bershady: *Professor of Astronomy at University of Wisconsin – Madison*. Main science interests are extragalactic astronomy and observational cosmology; galaxy kinematics, image structure, stellar populations; galaxy and quasar evolution; and optical and IR observations and instrumentation.

David Buckley: *Astronomer at South African Astronomical Observatory, Project Scientist of SALT*. Main science interests are time resolved simultaneous UV-Vis-NIR observations (spectroscopy & spectropolarimetry) of CVs, including magnetic & non-magnetic systems, and LMXBs; UV-Vis-NIR observations of exoplanet transits; and spectropolarimetry of GRBs.

Edward Churchwell: *Emeritus Professor of Astronomy at University of Wisconsin – Madison*. Main science interests are star formation, hot molecular cores, UC HII regions, atomic abundances, and radio and IR astronomy.

Steve Crawford: *SALT Science Data Manager at South African Astronomical Observatory*. Main science interests are observational cosmology and the evolution of galaxies, faint galaxy counts, starburst galaxies , luminous compact blue galaxies, clusters of galaxies, galaxy photometry, galaxy morphology, and instrumentation and spectrograph design.

Rob Fesen: *Professor of Astronomy at Dartmouth College*. Main science interests are supernovae and supernova remnants, the interstellar medium, shock waves, and Wolf-Rayet stars.

Jay Gallagher: *Professor of Astronomy at University of Wisconsin – Madison*. Main science interests are multi-wavelength observational investigations of evolutionary processes in galaxies, stellar populations, and classical novae.

Eric Gawiser: *Assistant Professor of Physics & Astronomy at Rutgers University*. Main science interests are galaxy formation and evolution, galaxy properties from multi-wavelength data.

Amanda Gulbis: *SALT Astronomer at South African Astronomical Observatory*. Main science interests are asteroids and KBOs.

Eric Hooper: *Assistant Faculty Associate in Physics and Lecturer in Astronomy at University of Wisconsin – Madison*. Main science interests are multi-wavelength studies of quasars, quasar environments, and obscured AGN.

John Hughes: *Professor of Physics & Astronomy at Rutgers University*. Main science interests include early type galaxies in clusters at $1 < z < 1.6$ and galactic supernova remnants.

Janusz Kaluzny: *Professor at Nicolaus Copernicus Astronomical Center, Warsaw, Poland*. Main science interests are LMXRB and binary brown dwarfs.

Sheila Kannappan: *Assistant Professor of Physics & Astronomy at University of North Carolina*. Main science interests are galaxy dynamics and evolution.

Alexei Kniazev: *SALT Astronomer at South African Astronomical Observatory*. Main science interests are star-forming galaxies, HII regions, planetary nebulae, and mergers.

Felipe Menanteau: *Postdoctoral Fellow in Astronomy at Rutgers University*. Main science interests include faint galaxies at $z > 0.5$.

Anand Narayanan: *Postdoctoral Fellow in Astronomy at University of Wisconsin – Madison*. Main science interests include quasar absorption line systems.

Kenneth Nordsieck: *Emeritus Professor of Astronomy at University of Wisconsin – Madison; Principal Investigator of RSS-VIS*. Main science interests are geometric and magnetic field diagnostics of circumstellar and interstellar matter through high spectral-resolution visible and infrared wavelength spectropolarimetry.

Steve Potter: *Astronomer at South African Astronomical Observatory*. Main science interests include polarimetry of magnetic CVs.

Blair Savage: *Emeritus Professor of Astronomy at University of Wisconsin – Madison*. Main science interests are physical properties of the interstellar medium, gas in galactic halos, and the intergalactic medium; high resolution ultraviolet spectroscopy.

Michael Shara: *Curator of Physical Sciences at American Museum of Natural History*. Main science interests are surveying the 100,000 stars nearest to Earth, local dark matter, globular clusters, blue stragglers, and emission line stars.

Andrew Sheinis: *Assistant Professor of Astronomy at University of Wisconsin – Madison; Principal Investigator of RSS-NIR*. Main science interests are the relationship between SMBHs and their host galaxies in the context of galaxy formation and evolution, triggering mechanisms of quasars, the relationship between the stellar environments in QSO hosts compared to quiescent galaxies, and what happens to the SMBH in galaxy interactions and collisions.

Linda Sparke: *Professor of Astronomy at University of Wisconsin – Madison*. Main science interests are measuring the motion of stars and gas in and around galaxies to probe the gravitational potential and dynamical history; and using emission and absorption lines from stars and gas to probe the star formation history.

Christy Tremonti: *Assistant Professor of Astronomy at University of Wisconsin – Madison*. Main science interests are feedback from stars and black holes, and galactic chemical evolution

Petri Vaisanen: *SALT Astronomer at South African Astronomical Observatory*. Main science interests are the nearby universe: strongly star-forming galaxies, interacting galaxies, AGN; higher redshifts: clusters out to z~0.6.

Jorick Vink: *Senior Research Astronmer at Armagh Observatory – UK.* Main science interests are mass loss and stellar cosmology, circumstellar geometries around young stars, horizontal branch stars, and the Halpha Survey of the Northern Galactic Plane (IPHAS).

Beverly Wills: *Research Scientist in Astronomy at University of Texas – Austin (HET consortium)*. Main science interests are active galactic nuclei from radio to x-ray wavelengths.

Marsha Wolf: *Assistant Scientist in Astronomy at University of Wisconsin – Madison*; *Project Scientist of RSS-NIR.* Main science interests are galaxy formation and evolution: quasar hosts and E+A galaxies as phases of galaxy evolution, stellar populations in galaxies, and disentangling age and metallicity estimates.

4 Optimizing the RSS-NIR Instrument Modes

4.1 Instrument Overview

From the beginning, the optical RSS on SALT has envisioned an additional NIR arm. This extension of the instrument, RSS-NIR, will be the first NIR instrument on SALT, expanding the capabilities of the telescope into an entirely new regime. With the exception of X-shooter on the VLT, the combined RSS will be unique among instrumentation for 8-10 meter class telescopes in its ability to simultaneously record data in the UV-visible and NIR. It will open a new window for the discovery and study of the most distant and earliest galaxies in the universe. The RSS-NIR upgrade will include a number of operational modes over the λ = 0.9 to 1.7 μm wavelength range: imaging, very high throughput low to medium resolution spectroscopy, narrow-band Fabry-Perot imaging, and spectropolarimetry. All modes will exploit the instrument's large 8 arcmin field of view. The design incorporates an articulated camera, volume phase holographic (VPH) gratings, and a single-etalon Fabry-Perot system. This instrument leverages the considerable effort and expense undertaken by UW researchers and others for the visible system, while preserving all of the visible capability. The design philosophy for RSS-NIR was to duplicate the capabilities of the visible side where possible, with any necessary adaptations for operation in the NIR. **Table 1** lists the main RSS-NIR instrument parameters.

Table 1. RSS-NIR instrument parameters.

Optical	
Telescope Aperture	11 meters
Telescope focal ratio	f/4.18
Collimator Focal Length	302 mm
Camera Focal Length	220 mm
Image space F/#	1.4289
Efl	15718.39 mm
Plate scale	76.205 μm/arcsec
Plate scale	4.233 pixels per arcsec (18 μm pixels)
Image Quality	Pixel limited in all modes , 2 pixels =0.5 arcsec
Field of View	8 arcmin dia (imaging), 8 x 8 arcmin (spectroscopic)
Spectroscopy	
Wavelength Coverage	0.9 – 1.7 μm, $\Delta\lambda$ = 0.8 μm
Gratings	4 articulated VPHGs, 1 conventional low R grating
Spectral Resolution	800, 2000-7000 (1arcsec slit)
Free Spectral Range (FSR) in one grating setting	FSR ~ 0.13 μm @ R ~ 2000 FSR ~ 0.11 μm @ R ~ 4000 FSR ~ 0.09 μm @ R ~ 7000 R~800 conventional grating to cover entire range, FSR = 0.8 μm
Pixel Scale	0.24
Field of View	8 x 8 arcmin
Multiplex	laser-cut MOS masks, up to 40 slits per mask
Throughput	45%, not including telescope
Detector	2048 x 2048 Teledyne Hawaii-2RG and ASIC, 18 μm pixels, long-wavelength cutoff @1.7 μm
Fabry-Perot Imaging	
Spectral Resolution	2500
Field of View	8 arcmin dia
Etalon Finesse	50
Order Blocking Filters	R ~ 50, 12 filters covering discrete atmospheric windows in J and H bands
Spectropolarimetry	
Polarization Measurements	linear, circular, all stokes
Instrument Modes	imaging, spectroscopy
Field of View	4 x 8 arcmin
Imaging	
Field of View	8 arcmin dia
Broadband Filters	Y, J, H

4.2 The NIR Night Sky

The NIR night sky is dominated by bright and variable OH emission lines that result in significant complications for astronomical observations. **Figure 2** shows a night sky spectrum from Maunea Kea in Hawaii. The locations of J and H band filters are indicated and the measured sky levels in these bands are marked with symbols for both the Maunea Kea and Sutherland sites (values from Taka Nagayama's thesis). High resolution NIR spectra of the night sky at the SALT site in Sutherland do not exist. Nonetheless, because the broadband measurements at the two sites are similar, we use the Maunea Kea spectrum to estimate the sky background for SALT.

4.3 Grating Spectroscopy

For faint objects at low spectral resolution, unresolved sky emission lines place the limit on the object magnitude that can be reached, independent of the telescope size or the instrument used. However, at higher spectral resolution the night sky lines are resolved and spectral features of astronomical objects can be observed down to the sky continuum between these lines. **Figure 3** shows an expanded scale sky spectrum smoothed to resolutions of R ~ 7000 (red) and R ~ 2000 (blue). At R < 4000 the majority of night sky lines are blended and observations cannot reach the true sky continuum between these lines over most of the spectral range. Our analysis shows that over the RSS-NIR spectral range of λ = 0.9 – 1.7

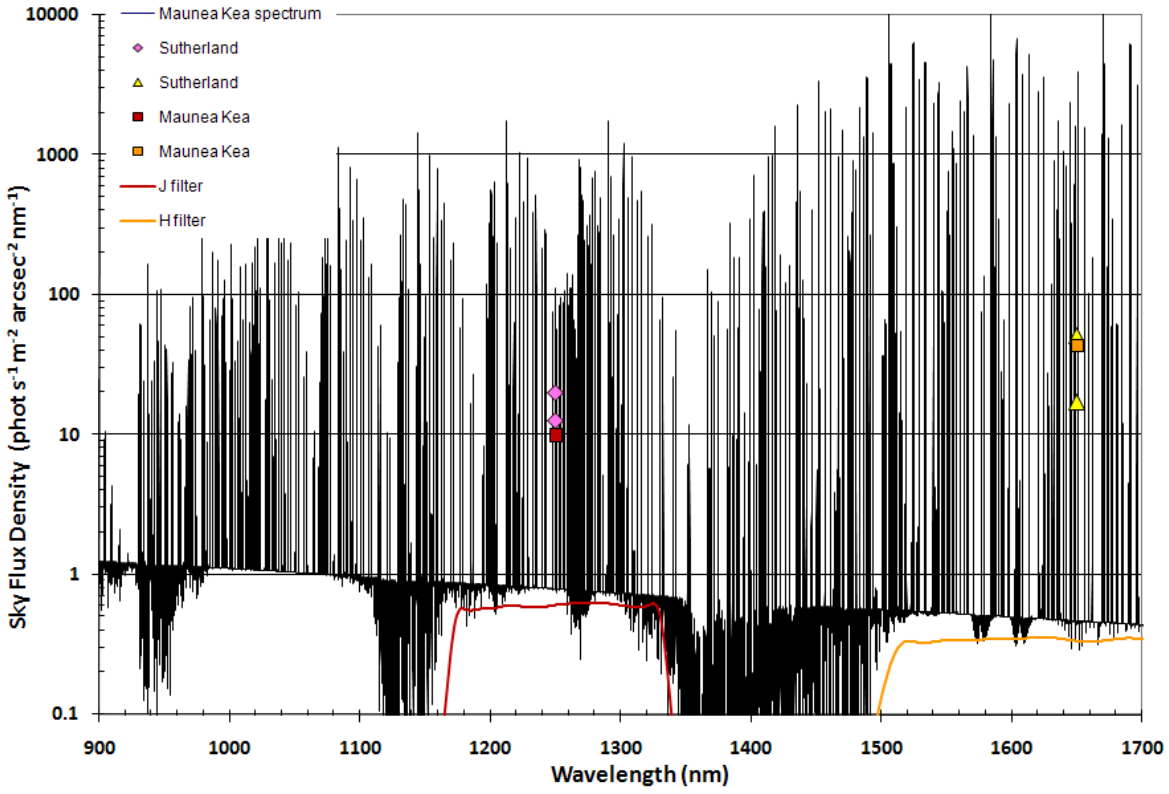

Figure 2. A spectrum of the NIR night sky from Maunea Kea, from the Gemini Observatory website. Observing conditions were airmass = 1.5 and H_2O = 1.6 mm with spectral resolution of $\Delta\lambda$ = 0.04 nm (R ~ 33750). The spectral locations of J and H band filter traces are shown for reference. Broadband sky levels in these bands for both the Maunea Kea and Sutherland sites are marked by symbols.

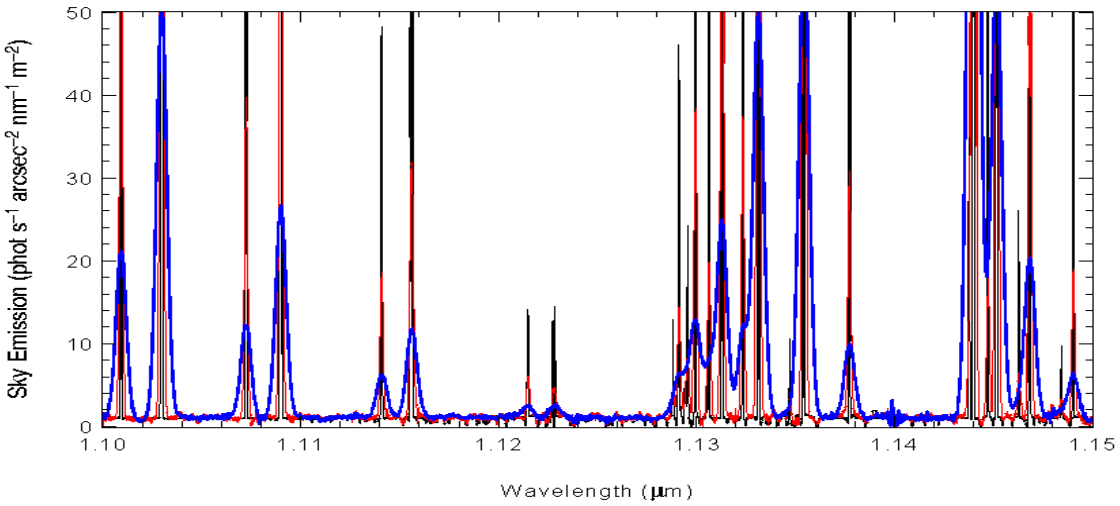

Figure 3. Night sky spectrum at different spectral resolutions. Underlying black is the original Maunea Kea spectrum at R ~ 33750, red is smoothed to R ~ 7000, and blue is R ~ 2000.

μm, at R=2000, 33% of the spectrum is free of sky emission lines; at R=4000, 47% is free; and at R=7000, 54% is free. Observations of faint objects should be made at R ≥ 4000 to achieve the true sky continuum limit within specific atmospheric windows between sky emission lines.

4.4 Fabry-Perot Narrow Band Imaging

The night sky emission lines similarly affect Fabry-Perot observations. Only objects with emission lines (intrinsic or redshifted) falling within atmospheric windows between sky emission lines can be observed without sky contamination. This means that, unlike the visible arm, the RSS-NIR Fabry-Perot will not require enough order blocking filters to cover the entire contiguous spectral range. Two kinds of observations are envisioned for the Fabry-Perot instrument: 1) observations of specific lines at z~0 in the ISM, nebulae, and star forming regions; and 2) searches for redshifted emission line galaxies. **Table 2** lists lines of interest that have been identified by SALT consortium astronomers, as well as the types astronomical objects in which they occur. The goal in selecting spectral locations of FP blocking filters is to choose the regions that are relatively free of night sky emission lines, but also to include important lines of interest at z=0, even if they lie close to a night sky line.

Table 2. Lines of interest and the types of objects in which they occur.

Wavelength (μm)	Element	Location		Wavelength (μm)	Element	Location
0.9069	[S III]	SF		1.26	[Fe II]	ISM, SN
0.91882	H-a, z=0.4	z search		1.28	Pa-b	ISM, SF
0.93175	[O II], z=1.5	z search		1.3126	H-a, z=1	z search
0.9532	[S III]	SF		1.3376	Ly-a, z=10	z search
0.9722	H-b, z=1	z search		1.43	[Si X]	nebula, AGN
0.9728	Ly-a, z=7	z search		1.4583	H-b, z=2	z search
0.9827	[C I]	nebula		1.4908	[O II], z=3	z search
0.9853	[C I]	nebula		1.5	Mg I	nebula

0.99	[S VIII]	AGN		1.5021	[O III], z=2	z search
1.0014	[O III], z=1	z search		1.5808	Ly-a, z=12	z search
1.0287	[S II]	SF		1.588	Br 14-4	H II regions
1.0321	[S II]	ISM, SF		1.611	Br 13-4	H II regions
1.0395	[N I]	SF		1.63	CO(6,3)	supergiants
1.0401	[N I]	SF		1.64075	H-a, z=1.5	z search
1.07	[Fe XIII]	AGN		1.641	Br 12-4	H II regions
1.08	He I	ISM, nebula		1.644	[Fe II]	ISM, SN
1.1181	[O II], z=2	z search		1.65231	[O III], z=2.3	z search
1.12	O I	nebula		1.65274	H-b, z=2.4	z search
1.25	[S IX]	AGN		1.68	Br 11	H II regions

One of the strongest science drivers for this operational mode from UW astronomers requires a spectral resolution of R ~ 2500 (see Section 6.1). For an etalon Finesse of 50, this leads to order blocking filters with R ~ 50, or an average spectral width of 0.027 μm. **Figure 4** shows a plot of the NIR night sky spectrum with preliminary locations of a set of 12 FP order blocking filters (12 is the number of filters available in the instrument at one time, though they are exchangeable). The black spectrum is the night sky from Maunea Kea that has been used throughout all our analyses. The cyan line near the bottom marks a factor of 2 above the sky continuum. Any spectral regions with a width of 5 etalon linewidths (so that 5 etalon settings could occur) that contain no sky lines above the cyan line are marked by small red dashes. (The y-axis level of these dashes are offset with wavelength for clarity to see individual marks.) These are line-free regions of the spectrum. The blue spectrum near the top is the atmospheric transmission, which has to be considered as well when selecting observing windows. The vertical green lines mark the locations of the spectral lines in **Table 2**. The thick horizontal magenta lines mark possible filter locations. Because the free spectral range of the etalon changes with wavelength, so do the widths of the filters. This is only a preliminary set of filters to demonstrate our selection process, as more analysis of the effects of the large wings on the etalon transmission lineshape is forthcoming.

4.1 Spectropolarimetry

Unlike spectroscopy, many spectropolarimetric programs will favor a lower dispersion, with higher spectral coverage. There are two reasons, one that many programs want very high S/N, and are going to a large telescope to get more photons: these objects are not at the sky limit, so high dispersion is not required to get around the sky lines. The other is that a wide spectral coverage is required to separate different polarimetric effects by wavelength dependence, like electron scattering and dust. In order to cover the entire NIR spectral range, a grating with R~800 will be required. This would likely have to be a conventional transmission grating or grism, as the volume phase holographic gratings do not perform well in this low dispersion regime.

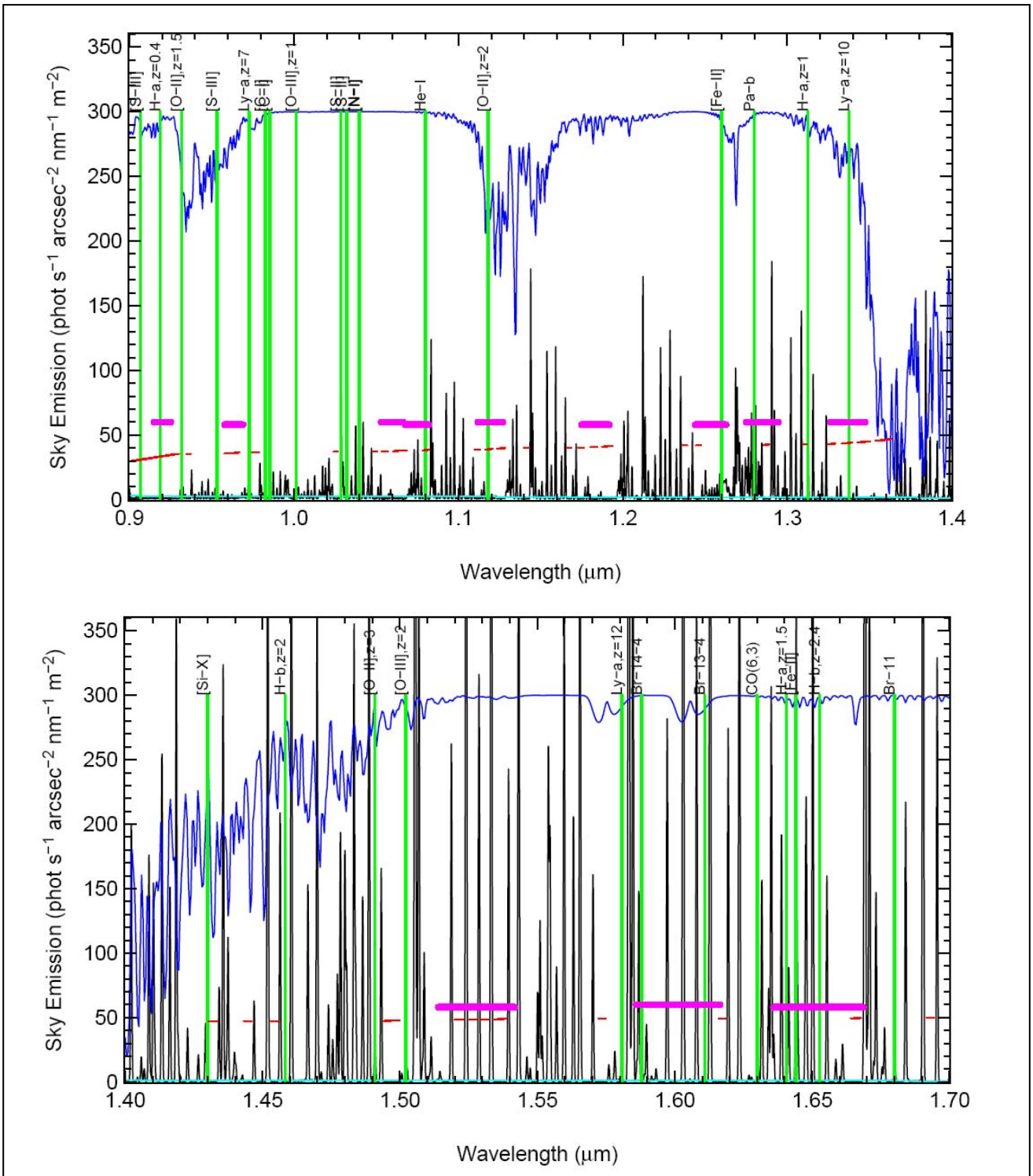

Figure 4. Preliminary locations of FP order blocking filters. See text for description.

4.2 Simultaneous Vis-NIR Observations

RSS will be unique in its ability to observe simultaneously with both the VIS and the NIR arms in all instrument modes: spectroscopy, Fabry-Perot narrow band imaging, and spectropolarimetry. There are a number of advantages to simultaneous observations, both technical and scientific in nature. First of all is the gained efficiency in obtaining both observations at once in cases where each instrument would normally be used sequentially to gain wider spectral coverage, or to observe two specific spectral regions falling in both the visible and the NIR. *With SALT's limited track times on objects this becomes a very important aspect for observing efficiency.* Simultaneous observations actually gain more than a factor of ~2 in efficiency when weather and possible downtime due to technical problems are considered. The likelihood of getting one good observation is better than the likelihood of getting two at different times.

Since both arms of RSS use a common slit plane, both instruments see the same spatial sampling. This is important for studies that need to precisely compare the visible and NIR observations of particular regions of objects, such as polarimetry or abundance studies, where observations obtained on different instruments or with different setups might not spatially sample the object in exactly the same locations.

Wide spectral coverage will be important for projects such as searching for spectral break in galaxies. Because the VIS and NIR arms of RSS are individually configurable, we will have great flexibility in possible observations. For example, we could consider searching for high redshift Ly-break galaxies by using the R = 300 grating on the VIS side, to cover its entire spectral range at once, and higher spectral resolution on the NIR side to get between the sky lines. Together the total spectral range covered is very wide.

Many of the spectropolarimetric observations will require wide spectral coverage at fairly low spectral resolution because they are bright sources. Objects that have intrinsic polarization are often variable, so this enforces the case for making simultaneous observations with both arms.

Some studies will require the observation of different features that are separated far enough in wavelength that they cannot be done by a single visible or NIR instrument. Some examples include nebular diagnostics (ionization, metallicity, extinction), particularly in redshifted sources; stellar population synthesis (age/metallicity), where a broad range in wavelength is needed to constrain both hot and cool stellar populations; and redshift identification and confirmation. All such studies will benefit from the gained observational efficiency of making both observations at once, as well as the stability of making both observations through the same weather conditions.

4.3 The Dichroic Split Between Arms

Both the wavelength at which the dichroic beamsplitter separates the light for the visible and NIR arms and the steepness of the cut are driven by science arguments. A shallow transition would provide more overlap between spectra from the two arms. However, virtually no science applications within the SALT consortium require much overlap between the visible and NIR arms when spectra are obtained simultaneously. Calibration of each arm will be done separately by observing spectrophotometric standards. On the other hand, spectropolarimetric observations prefer a sharp cut because coating

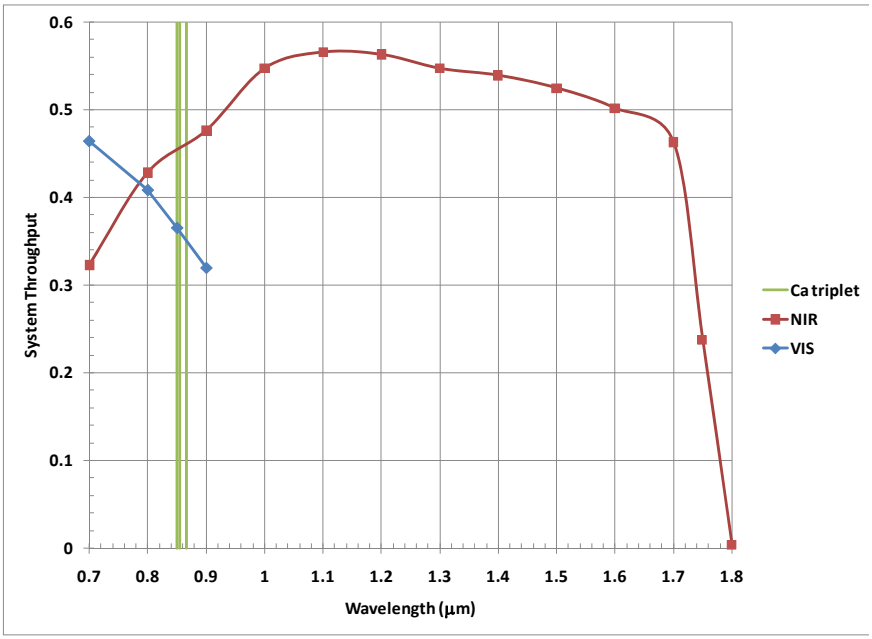

Figure 5. System throughputs for the VIS and NIR arms of RSS. The Ca IR triplet wavelengths are marked. Throughput crossover occurs just blueward of this feature.

properties of the dichroic vary with polarization and prevent the measurement of accurate polarizations near the cut wavelength.

The Ca IR triplet at λ = 8498 Å, 8542 Å, and 8662 Å is a spectral feature important to many science programs. One important aspect of the decision on exactly where to make the dichroic wavelength split is which system will be most efficient for observing this feature. **Figure 5** shows the estimated system throughputs of both the visible and the NIR arms of RSS. These include all optics, coatings, gratings, and detector QEs. The throughput crossover occurs just blueward of the Ca triplet. Operationally, it should not matter which arm is used to observe the feature since the thermal background is not an issue at this wavelength on the NIR side. An important scientific consideration is what other features are likely to be observed at the same time as the Ca IR triplet? This will be considered for the final decision on this exact wavelength. Nominally, the split will be at λ = 0.9 μm.

5 Comparison with Other Instruments

RSS-NIR fills an obvious gap in SALT instrumentation since it will be the first NIR instrument on the telescope. It is also important to compare the unique capabilities of RSS to instrumentation on large telescopes worldwide. **Table 3** lists the spectroscopic capabilities of NIR instruments on 4-11 meter class telescopes worldwide. Any extra instrument modes are noted in the last column. Of all NIR instruments on 4-11 meter class telescopes, RSS and X-shooter are the only two that can simultaneously cover the UV-VIS-NIR wavelength range. X-shooter does this routinely at the optimal design spectral resolutions. While RSS can observe at any of its instrument resolutions simultaneously in the VIS-NIR, it could only achieve contiguous coverage at low resolution, R~800. However, for X-shooter, detector real estate for spectral coverage comes at the price of observing only single objects. RSS has a wide field multi-object mode utilizing custom laser-cut masks with up to 40 slits per mask. Furthermore, the tunable VPHGs (in both wavelength region and spectral resolution) in each arm, in conjunction with multi-object slit masks, allow great flexibility in observations. For example, the gratings on each side could be tuned to observe both Hα and Hβ in a galaxy cluster at z=0.5 (refer to **Figure 1** for redshifted spectral features), or to simultaneously observe the star formation indicators Hα and [O II]. There are

many projects that will not require the entire contiguous spectral coverage, but where two discrete regions would be highly desired.

Table 3. Comparison of NIR instruments on 4-11 meter class telescopes worldwide.

Telescope	Instr.	Field of View	λ range (μm)	R (λ/Δλ)	# Objects	Pixel size (")	FSR in one setting (μm)	Limiting magnitudes Vega	Extra modes
SALT	*RSS-NIR* *RSS*	8'x8' 8'x8'	0.9 - 1.7 0.32 – 0.9	1000-7000	40	0.22	Δλ ~ 0.09 – 0.2 0.32 – 1.7 @ low R	H=19.8 (19.2), S/N=10, t = 1 hr, R=4000 (7000)	Fabry-Perot, Spectro-polarimetry
Gemini	*NIFS* ‡ *(AO)*	3"x3"	0.95 - 2.4	5000-6000	single IFU	0.04	z, J, H, or K	H=18.3, S/N=5, t = 1 hr	
	Flamingos-2	2'x6'	0.95 - 2.5	1200, 3000	MOS masks	0.18	0.9-1.8, 1.25-2.5 J, H, or K		Fabry-Perot†
Keck	*MOSFIRE*	6'x3'	0.97 – 2.45	3270	45	0.18	1.48-1.81, 1.97-2.42	H=20.1, S/N=10, t = 1000 s, R=3270	
	OSIRIS ‡ *(AO)*	2.2"x 3.2"	1.0 – 2.4	3900	391 fibers	0.02–0.1	Δλ ~ 0.06 – 0.4	H~21.1,** S/N=10, t = 1 hr	
Subaru	*MOIRCS* ‡	4'x7'	0.9 – 2.5	500, 1500-1600	40	0.117	0.9 – 2.5	H~18.4,** S/N=10, 1 hr, R=1600	
	FMOS	30'	0.9 – 1.8	500, 2200	400 fibers		0.9 – 1.8 @ R=500, 4 settings at R=2200	H=20.9, S/N=5, t = 1hr	
VLT	*X-shooter*	12" slit	0.3 – 1.9	5000	1	0.14-0.31	0.3 – 1.9	H=18.6, S/N = 10, t = 1 hr, R=5000	IFU*, Spectro-polarimetry *
GTC	*EMIR*	6'x4'	0.9 – 2.5	4000	45	0.2	0.9 – 2.5	H=21.1, S/N = 5, t = 2 hr, R=4000	
LBT	*Lucifer*	4'x3'	0.9 – 2.5	500-5000, 1000-10000	MOS masks	0.25, 0.12	Δλ = 0.46, 0.22		IFU*
Magellan	*FIRE*	7" slit, 1' slit	0.8 – 2.5	6000, 900-2500	1	0.18	0.89 – 2.51	J=20.0, S/N=10, t = 2.3 hr, R=6000	

Telescope	Instr.	Field of View	λ range (μm)	R (λ/Δλ)	# Objects	Pixel size (")	FSR in one setting (μm)	Limiting magnitudes Vega	Extra modes
MMT	*ARIES*	107"	1 – 5	2000, 30000	MOS	0.1	J,H, and K J-H, H-K	J=20.7 (18.5) S/N = 10, t = 1hr, R=2000 (30000)	

‡, instrument in operation, † planned upgrade, * possible upgrade option, ** our estimate

We define an instrument comparison metric here that attempts to quantify the amount of information collected in a single instrument observation (Bershady et al., astro-ph/0403478). We plot the product of the telescope size and instrument field of view, AΩ (m^2 $arcsec^2$) against the spectral power, defined as the product of spectral resolution (λ/Δλ), number of spectral resolution elements in one setup ($N_{\Delta\lambda}$), and the number of objects observed in the setup (N_{obj}). This comparison for the instruments listed in **Table 3** is shown in **Figure 6**. RSS-NIR wins on AΩ with the exception of FMOS on Subaru.

We also adopt a performance metric from the X-shooter team, the "power" of a spectrograph. This metric is defined as $P = R\,(\lambda_2/\lambda_1)\,/\,t$, where *R* is the spectral resolution (λ/Δλ), λ_2 is the longest wavelength of the free spectral range (FSR) of one setting, λ_1 is the shortest wavelength of the FSR, and *t* is the time in sec to reach S/N=10 $Å^{-1}$ for a H_{AB}=19.5 object. Values are given in **Table 4** for the instruments for which we have enough information to scale the predicted observations. The last two columns give the power for a single object and for multi-object spectroscopy (MOS). The AO instruments have been excluded. At R~4000 RSS-NIR for observing a single object has a P = 6.6, while X-shooter is at P = 6.9 for R~5000. If we consider the MOS mode of RSS-NIR where 40 objects can be multiplexed, the power goes up to P = 263.

Table 4. Comparison of spectrograph power.

Telescope	Instrument	Resolution	Time (s)	P (single)	P (MOS)
SALT	RSS-NIR	2000	902.39	2.52	100.89
	RSS-NIR	4000	652.17	6.58	263.21
	RSS-NIR	7000	1125.45	6.74	269.67
Keck	MOSFIRE	3270	127.52	31.36	1411.25
Subaru	MOIRCS	1600	21493.27	0.21	8.27
VLT	X-shooter	5000	4586.19	6.90	6.90
GTC	EMIR	4000	524.93	21.17	952.50
Magellan	FIRE	6000	6698.35	2.53	2.53
MMT	ARIES	2000	7219.09	0.58	3.48
	ARIES	30000	1846.29	23.14	138.83

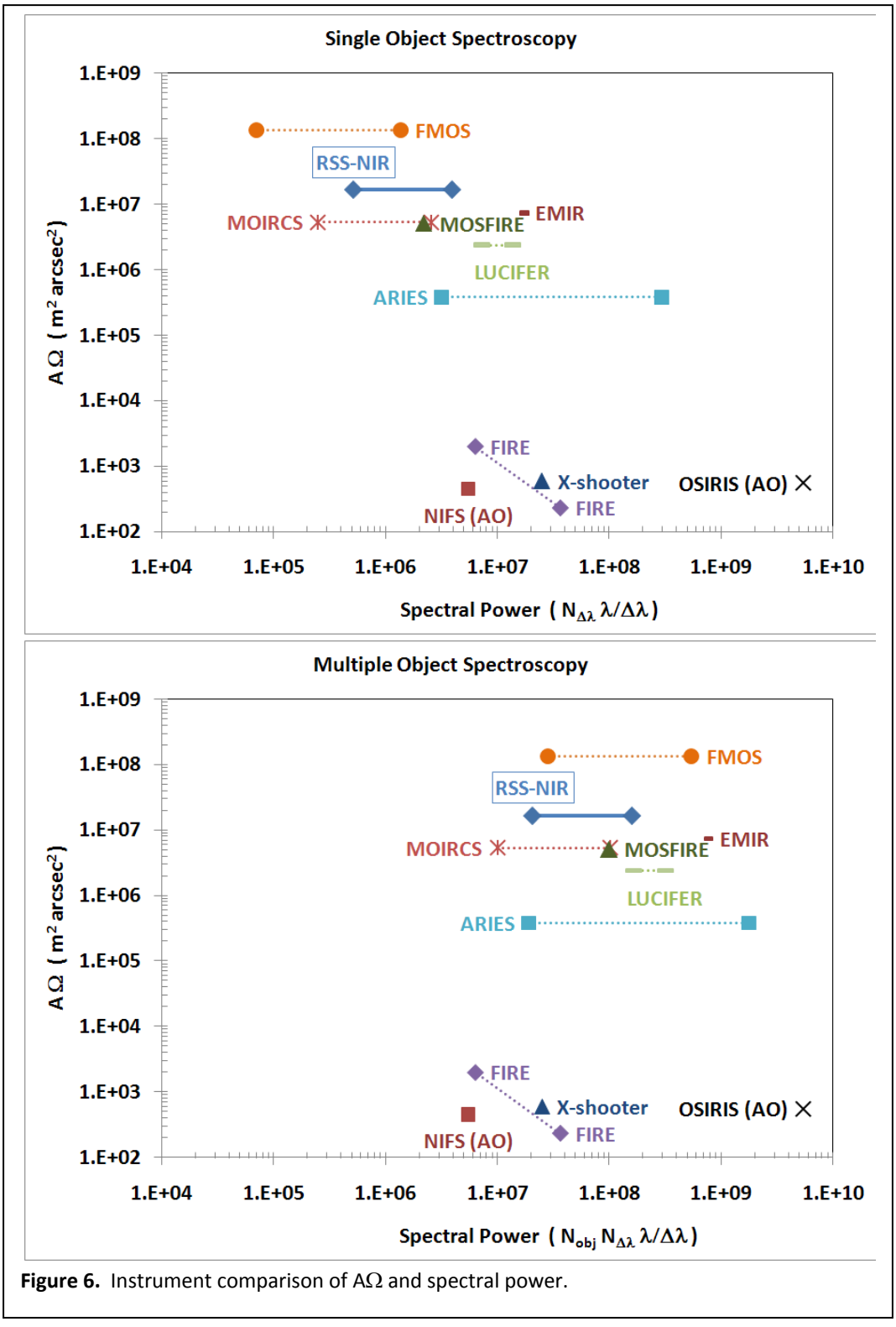

Figure 6. Instrument comparison of AΩ and spectral power.

5.1 RSS-NIR Performance Predictions

We have designed RSS-NIR to optimize high throughput, which has led our choices to: volume phase holographic gratings (VPHGs) for an increase in efficiency over conventional gratings, all transmissive optics with efficient AR coatings (we are investigating hardened solgel), and a HAWAII-2RG detector for which arrays have demonstrated quantum efficiency > 0.8 over our entire operating wavelength range. Preliminary throughput predictions of RSS-NIR are shown in **Figure 7**.

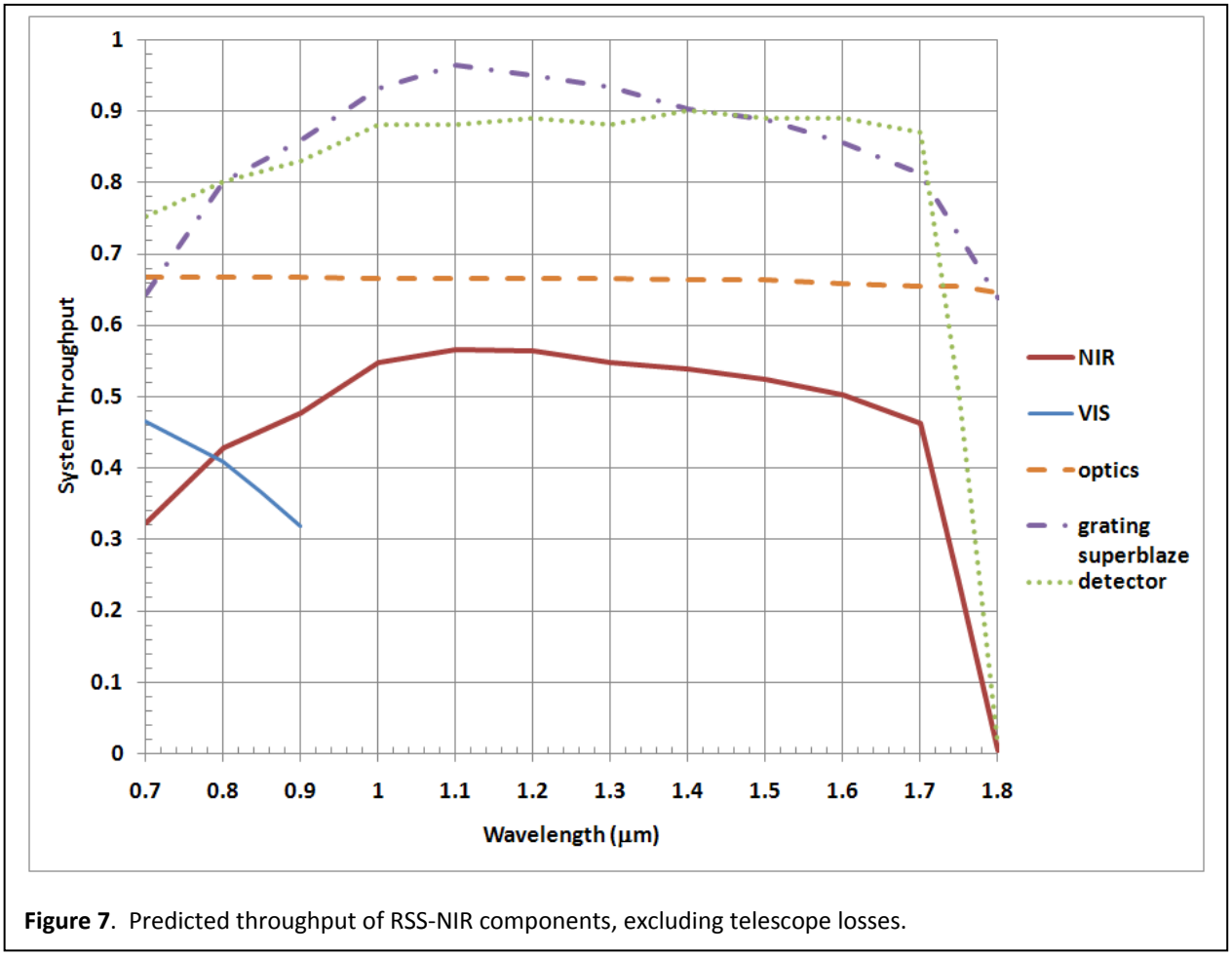

Figure 7. Predicted throughput of RSS-NIR components, excluding telescope losses.

We have developed a sky-limited performance model for RSS-NIR that uses actual material transmissions of all optics, predicted volume phase holographic grating efficiencies (using the Kolgelnik approximation), and a detector quantum efficiency spectrum for a Hawaii-2RG-1.7µm array from Teledyne (Beletic et al. 2008). The instrument thermal backgrounds used in this model were determined from actual ray traces in a detailed thermal stray light analysis, which has been integral to the design of this instrument (see RSS-NIR Thermal Stray Light Analysis document SALT-3501AA0002). We have assumed a worst case of 5 "dirty" telescope mirrors with $R_{primary}$ = 0.89 and each of the 4 spherical aberration corrector (SAC) mirrors at R_{SAC} = 0.96. Resulting performance predictions for RSS-NIR are given in **Table 5**, **Figure 8**, and **Figure 9**. These are limiting Vega magnitudes to reach S/N = 10 per resolution element in a 1 hour exposure for 1 arcsec^2.

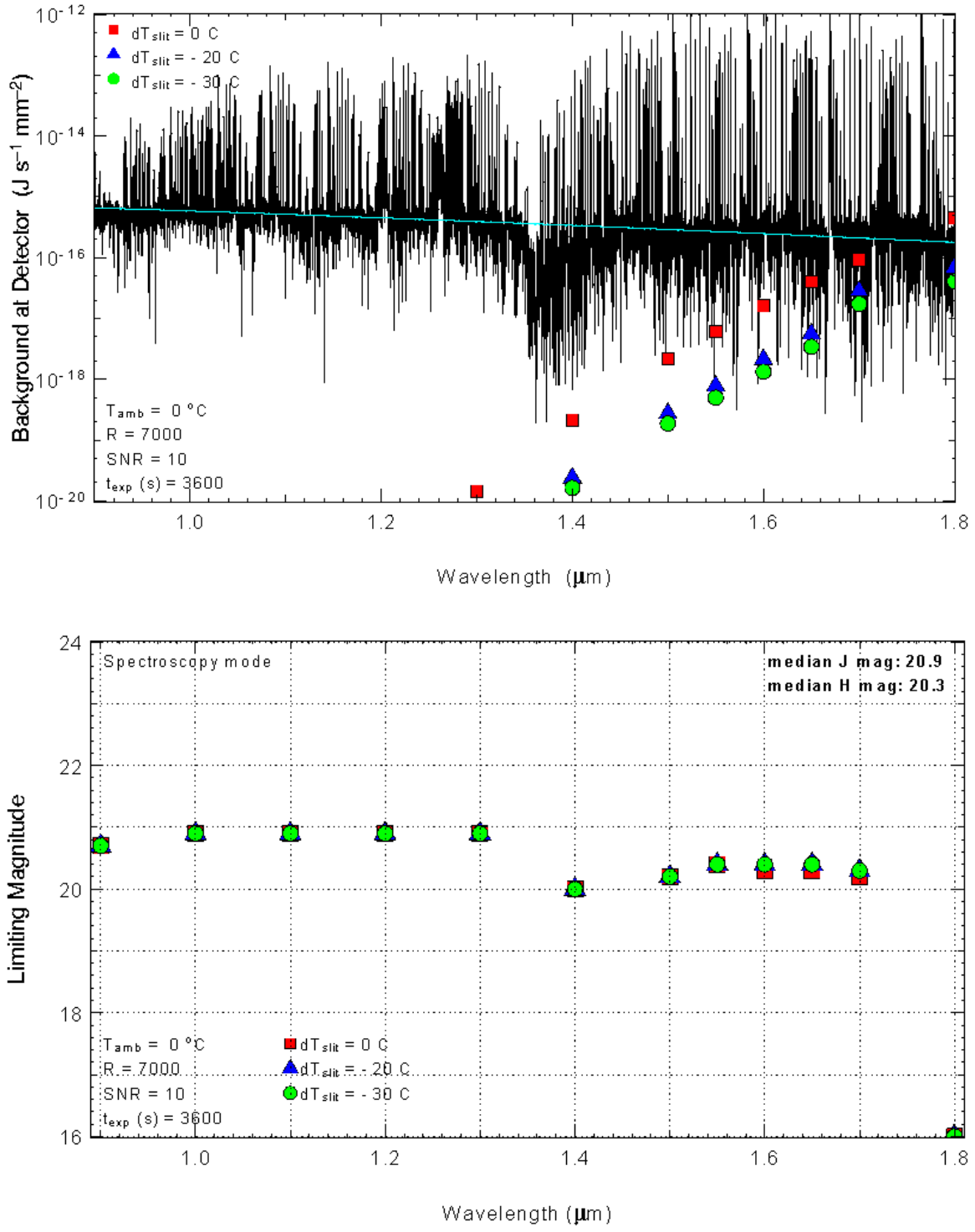

Figure 8. RSS-NIR performance predictions. The top plot shows the background flux density at the detector for R=7000 and T_{amb} = 0 °C. The black spectrum is the sky, and the symbols are the instrument background for no slit cooling (red squares), dT_{slit} = -20 °C (blue triangles), and dT_{slit} = -30 °C (green circles). The bottom plot shows the limiting Vega magnitudes to reach S/N=10 per spectral resolution element in a 1 hour exposure for 1 arcsec^2 as a function of wavelength.

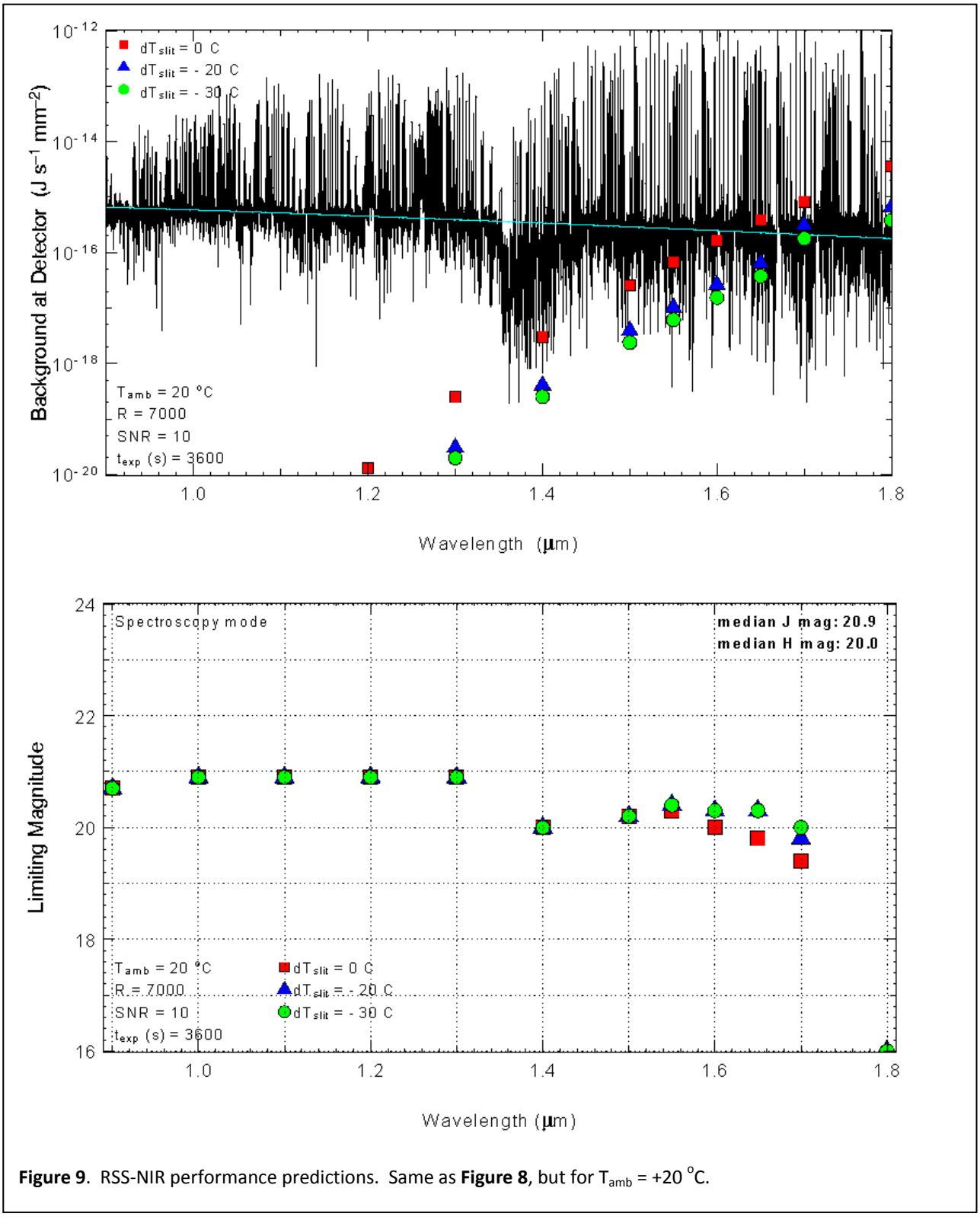

Figure 9. RSS-NIR performance predictions. Same as **Figure 8**, but for T_{amb} = +20 ^{o}C.

Table 5. RSS-NIR limiting magnitude performance predictions for S/N = 10 per resolution element in 1 hour for 1 arcsec^2.

Spectral Resolution (R)	Ambient Temperature (^{o}C)	Slit Cooling below Ambient (^{o}C)	Limiting J mag Vega (AB)	Limiting H mag Vega (AB) to 1.7 μm
4000	0	0	21.1 (22.0)	20.1 (21.5)
4000	0	-20	21.1 (22.0)	20.1 (21.5)
4000	0	-30	21.1 (22.0)	20.1 (21.5)
7000	0	0	20.7 (21.6)	19.6 (21.0)
7000	0	-20	20.7 (21.6)	19.6 (21.0)
7000	0	-30	20.7 (21.6)	19.6 (21.0)
4000	20	0	21.1 (22.1)	19.8 (21.2)
4000	20	-20	21.1 (22.1)	20.0 (21.4)
4000	20	-30	21.1 (22.1)	20.0 (21.4)
7000	20	0	20.7 (21.6)	19.2 (20.6)
7000	20	-20	20.7 (21.6)	19.5 (20.9)
7000	20	-30	20.7 (21.6)	19.5 (20.9)

Two different cases are shown. In **Figure 8** the top plots shows the flux density of the backgrounds reaching the detector for R=7000 and an ambient temperature of T_{amb} = 0 ^{o}C as a function of wavelength. This represents a cold winter night, with the median SALT winter temperature at +3 ^{o}C. The black spectrum is the sky (using a Maunea Kea sky observation), the cyan line is a fit to the sky continuum, and the symbols are the instrument backgrounds. The different symbols represent different amounts of slit cooling below the ambient observatory temperature: none (red squares), dT_{slit} = -20 ^{o}C (blue triangles), and dT_{slit} = -30 ^{o}C (green circles). These plots are instructive to see at what wavelength the instrument thermal background due to self emission begins to dominate the sky background. The bottom plot shows the limiting Vega magnitude as a function of wavelength. **Figure 9** shows the same plots for T_{amb} = +20 ^{o}C, the maximum typical summer temperature, with the summer median at T_{amb} = +13 ^{o}C. **Table 5** also gives limiting magnitudes for R=4000 under the same conditions. The minimum spectral resolution that we discuss here is R = 4000, because below that resolution the observed spectrum becomes dominated by night sky emission lines that are no longer resolved. Sky-limited observations of faint objects cannot typically be done at R < 4000. Objects that are much brighter than the sky could be observed at lower spectral resolution, however, for them these limits due to backgrounds will not be an issue.

6 The Processing of Baryons in Galactic Systems

This project was presented as the science case in our successful NSF MRI proposal for RSS-NIR, and remains a high priority program for the University of Wisconsin science team.

6.1 Ultra-High Redshift Universe: Discovering First Light

> Discover when and how rapidly the first galaxies formed. When is reionization complete? The frontier is z > 7. The achievable flux limit for SALT is about z = 10.

The new frontier in extragalactic astronomy and cosmology lies at z > 7, when the universe emerged from a period known as the "cosmic dark age." This epoch is marked by the formation of the first (Pop III) stars in proto-galactic units, i.e., "First Light." The details of this primordial processes remain murky and observations are sparse. The theoretical picture of early hierarchical build-up of galaxy mass, modulated by gas physics, is still beyond the grasp of accurate modeling. In particular, as baryons in the comic web began to dissipate into galactic potentials, it is unclear how rapidly star-formation began, and over what range of mass potentials. *Measuring the onset of star-formation and the luminosity function (LF) of the first star-forming galaxies would consolidate our theoretical framework, particularly if mass estimates could also be made. With RSS-NIR we will make such a measurement.* The observational approach is challenging because the key diagnostic, Lyα, is shifted beyond 1 μm (the end of the optical window) at z > 7. The universe at these early times remains largely neutral since sources of ionizing radiation were rare and hence essentially opaque to photons with rest wavelength below the Ly limit, 912 Å (the Gunn-Peterson

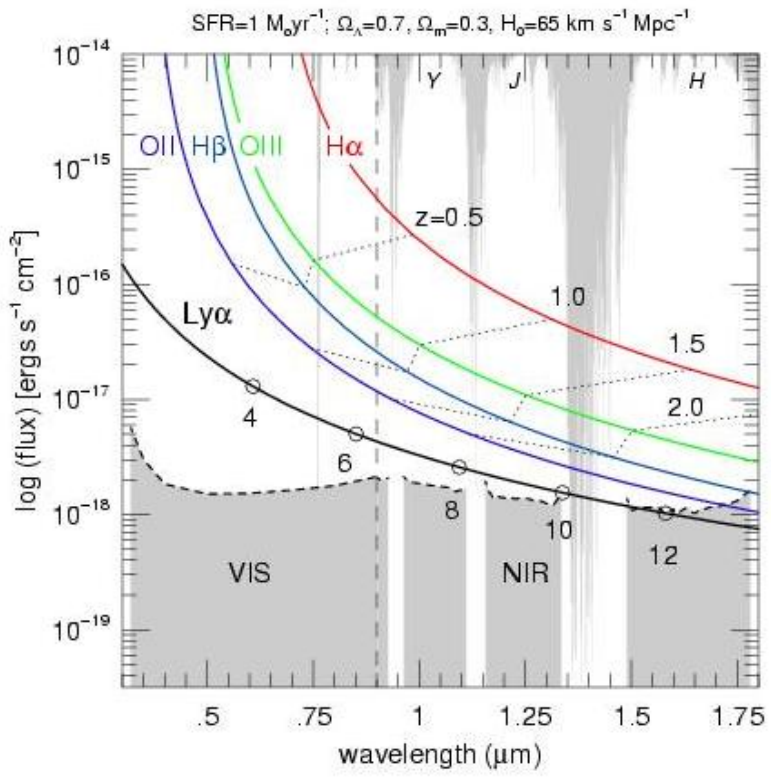

Figure 10. Sensitivity limits for 5σ emission-line detection in a 1 hr exposure at R = 4000 within 1 arcsec^2 for the RSS visible (VIS) and NIR beams (grey areas and dashed curves). Limits correspond to regions between sky-lines, ~40-60% of the NIR band-pass in J and H at this resolution. Atmospheric extinction is also shown. Labeled redshift tracks for Lyα through Hα for a galaxy forming 1 M$_\odot$ yr^{-1} of stars. This shows that we can detect sources with modest SFR in Lyα to z = 12. Other nebular diagnostics are easily detectable at lower redshift, thus opening SF and abundance studies to more quiescent galaxies to z = 2.5.

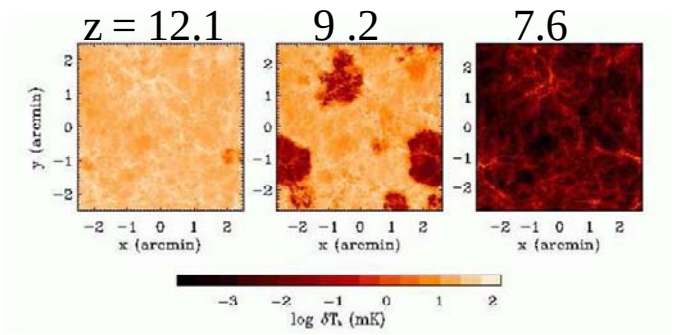

H I brightness temperature: Reionization (Furlanetto et al.)

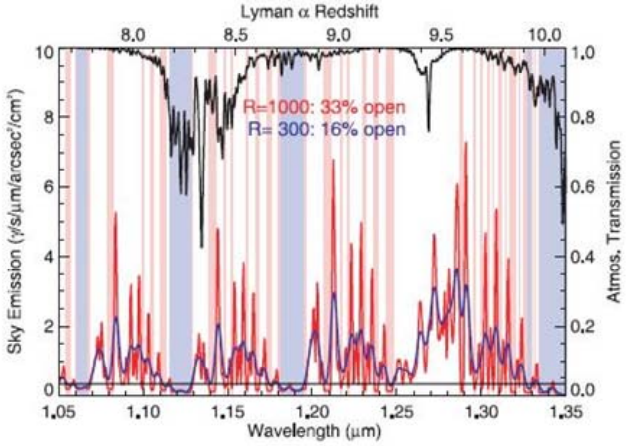

Lyα redshifts relative to bright sky emission features.

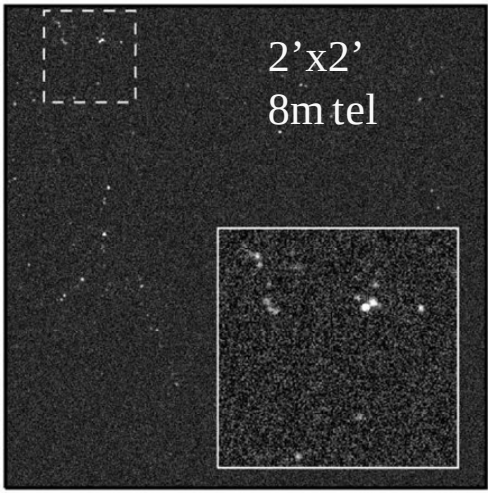

Lyα In the *J* band. (Barton et al. 2004)

Figure 11. Simulations of first light objects.

effect). The future of high-redshift science therefore lies in the near-IR.

Approach: The path to discovering the First-Light epoch is with a blind survey with sufficient sensitivity and survey volume to detect Lyα emission at least down to star-formation rates (SFR) comparable to that of normal galaxies like the Milky Way today (a few $M_\odot$ yr^{-1}).[1] The most sensitive programs proposed to date have focused on infrared narrow-band approaches (see Nilsson et al. 2007 for a summary) because of their ability to sample large volumes. However, all require intensive spectroscopic follow-up to eliminate lower-redshift interlopers posing Hα, [OIII] or [OII] emission-lines into the band-pass. Our approach follows the narrow-band scheme, but uses our unique dual-beam Fabry-Perot design to simultaneously eliminate interlopers.

Feasibility: To routinely detect Lyα emitters at or below the knee of the luminosity function at z = 10, we will have to reach sensitivity limits of about 10^{-18} ergs s^{-1} cm^{-2}. This is consistent with extrapolating the Lyα LF measured at z = 5.7 or z = 6.5, or attempts to model the possible distribution of Lyα luminosities at higher redshifts (see, e.g., Fig. 4 of Nilsson et al. 2007). As shown in **Figure 10**, we expect that Fabry-Perot searches with RSS will allow us to reach these very deep sensitivity limits; we can detect a Lyα galaxy with a SFR as little as 1 $M_\odot$ yr^{-1} in a 1 hr exposure. These sources are

[1] Lyα will scatter on the neutral IGM, but First Light is also the epoch of re-ionization, therefore, discovery of a Lyα luminosity function down-turn is effectively First Light.

expected to be < 1 arcsec in size.

Experimental design: To establish the Lyα LF requires at least ~30 galaxies at a given epoch. We will scan the regions in the NIR spectrum lying between the OH emission lines, using the entire 8' etalon field (50 arcmin^2) since we can accept a band-pass range in a blind survey. Two opposing considerations constrain the optimum etalon resolution: line- and volume-sensitivity. At lower resolutions, survey volume is increased at the sacrifice of line-sensitivity. We choose R = 2500 (sensitivity limits at R = 4000 in **Figure 10** are similar) to optimize line-sensitivity for intrinsic Lyα widths of σ = 50 km s^{-1}, typical of low-mass objects. This resolution is 2-4 times higher than other surveys, and allows us to take unique advantage of the likely steep Lyα LF at First Light. Further advantages are noted below.

The total required survey time will depend strongly on redshift as we approach First Light, and hence we will move out systematically in redshift to guarantee a positive result. Based on Nilsson et al.'s (2007) predictions, we require 12 x 1hr fields (or 12 etalon steps in one field) at z=8 to detect 30 sources (3800 sources deg^{-1} per 0.1 Δz), which is a modest program. At z = 9 and 10, 53 and 1600 hr would be anticipated to detect a comparable number of sources. The extent of the survey in redshift will depend, therefore, on our initial results, but can be extended by using foreground clusters as a lensing-boost (e.g., Scott et al. 2006). In addition to the single etalon, this requires only a few order-blocking filters sampling line-free regions in the Y, J and H bands.

Eliminating interlopers: We take advantage of high resolution and unique, simultaneous optical coverage by (a) identifying Lyα lines from their unique asymmetric profile; (b) rejecting Hα interlopers by scanning the matching [OII] line in the visible; (c) rejecting [OII] by scanning a minimum of 5 consecutive wavelengths in the NIR to split the 3726-3729A doublet; and (d) rejecting [OIII] and Hβ by scanning three sets of wavelengths separated by the redshifted [OIII]- Hβ spacing.

Spectroscopic follow-up: An additional advantage of our etalon resolution and experimental design will be measured line-profiles and hence mass-estimates of the First Light Lyα emitters. If sources are unresolved (an interesting result), we will follow up sources in VPH-grating multi-slit mode using the same optical system.

6.1.1 Instrument Requirements

- FP imaging R = 2500 to z = 10 (1.35 μm).
- Extension to 1.65 μm allows detection out to z = 12-13, but SFR will have to be few $M_\odot$ yr^{-1} -- unknown: *high-risk / high-return.*
- Simultaneous optical FP to cull interlopers (tune to redshifted [OII]3727 if NIR-line is Hα).
- Follow-up optical-NIR MOS at R > 4000 to eliminate remaining interlopers (split [OII]3727 doublet), determine kinematics to make dynamical mass estimates, constrain winds and outflows.

6.2 Star-Formation in the "Desert:" When Galaxies Were Young

Map star-formation rate and dynamical masses using [OII]3727 in the 1.4 < z < 2.6 regime when most of the mass-assembly for massive galaxies is believed to have taken place.

The era when *massive* galaxies have already assembled most of their mass and formed most of their stars is expected to be near z ~ 2, but there is considerable observational uncertainty in our knowledge. The pace of baryon dissipation in this growth is an important test of hierarchical galaxy formation models, particularly when coupled to a measurement of First Light, which also involved the precursors of these most massive systems. *The key observable diagnostics are the distribution of SFR with galaxy mass which we will measure with RSS-NIR.*

Figure 12. Young forming galaxies from the Hubble UDF.

Evidence from HST imaging indicates the traditional Hubble sequence (massive galaxies) is absent before z ~ 1.5, preceded instead by disturbed or small systems (van den Bergh et al. 1996). Independently, estimates for the co-moving star-formation history of the universe indicate a peak near z~1.5, or at least a down-turn after this epoch (Hopkins & Beacom 2006, and references therein). These observations, coupled with estimates of an elevated galaxy interaction and merger rate in the past (Ryan et al. 2007) paints a picture of an epoch where galaxies coalesce and settle into their present-day morphological types. The z ~ 2 regime appears a critical transition epoch in the history of galaxy evolution.

While significant resources have been devoted to the exploration of the "redshift desert" between 1.4 < z < 2.6, where [OII] has been redshifted out of the optical band-pass, but Lyα has not yet been shifted in, we don't have a detailed picture of the galaxy population in this regime. Optical surveys for these galaxies require ultradeep exposures on 8-10m class telescopes to identify weak metal absorption features against the galaxy starlight (Abraham et al. 2004, Steidel et al. 2004, Erb et al. 2006). However, with an efficient NIR spectrometer, one can directly observe the strong, rest-frame optical emission lines of these galaxies (Pettini et al. 2001).

Our particular focus will be to use RSS-NIR in VPH multi-slit mode to open [OII] emission-line surveys of galaxy SFR and line-widths (mass) from the present limit of z ~ 1.4 (e.g., DEEP and DEEP2) to the regime of existing Lyα surveys at z > 2.6. As Fig. 1 shows, RSS-NIR has sensitivity to [OII] emission well below SFR of 1 $M_{\odot}$ yr^{-1} to z ~ 2. We will capitalize on existing, deep imaging and optical spectroscopic surveys to study 1.4 < z < 2.6 sources, measure their [OII] SFR and infer their dynamical masses from kinematic line-widths.

6.2.1 Instrument Requirements

- Simultaneous optical-NIR MOS at R > 4000 out to 1.35 μm; resolution needed to optimize S/N, split [OII]3727 doublet, and estimate dynamical mass; OP/NIR needed to cull interlopers and acquire multiple lines for metallicity estimates and ISM diagnostics.
- Extension to 1.65 μm allows detection in [OII]3727 out to z=3.4 at SFR ≥ 1 $M_\odot$ yr^{-1} - well-beyond peak in comoving SFR and AGN activity.

6.3 Baryon Processing in a Mature Universe

> Precision mapping of the down-turn in the co-moving SFR and chemical enrichment from 0<z<1, as function of dynamical mass, using Hα and strong-line nebular diagnostics ([NII]/ Hα, [OIII]/ Hβ).

The dramatic down-turn in the co-moving SFR over the last Hubble-time is thought to represent a winding down of mass-assembly and the shifting of star-formation to lower-mass systems. The detailed transition remains uncertain because no single SF tracer has been available over the full redshift range 0<z<1. Furthermore, we know little about the detailed nebular abundances in galaxies beyond z > 0.5 because the strong lines required (Hα/[NII], Hβ/[OIII]; e.g., Salzer et al. 2005) are shifted out of the band-pass. (The weak-lined method involving [OIII]λ4363 is more precise but measurements preclude studies to very luminous or intensely star-forming sources.) Consequently we cannot watch reliably the growth of the mass-metallicity relationship that imprints today's galaxy distribution as well as the most luminous stellar populations we see today. *With RSS visible and NIR beams in dual multi-slit spectroscopic mode we will completely revolutionize our picture of this late phase of galaxy evolution by pinpointing Hα SFR and nebular abundances in systems with SFR as low as 0.1 $M_\odot$ yr^{-1} out to z=1.*

6.3.1 Instrument Requirements

- Simultaneous optical-NIR MOS at R > 4000 out to 1.35 μm; split[OII]3727 doublet and cull interlopers; acquire multiple lines for metallicity estimates and ISM diagnostics.
- R = 7000 for kinematics of narrow-lined (sigma<70 km/s) systems at the low-mass end.
- Extension to 1.65 μm allows detection of Hα out to z=1.5, well into the youthful regime for massive galaxies.

6.4 Star-formation at z = 0

> Constrain theories of star-formation that link production of elements and luminosity, to the energetics of feedback mechanisms and chemical enrichment which drive the evolution of baryons in galactic systems. Hα/Paβ flux ratios in obscured, star-forming regions and linear spectropolarimetry of circumstellar regions in obscured sources are the primary measurements.

The final piece of the dissipation puzzle is to constrain current theories of massive star formation at z=0. In order to do this we will characterize the circumstellar regions of young massive stars, using linear spectropolarimetry. This tool provides the possibility of probing the innermost regions around young

stars and exploring spatial scales that direct imaging techniques simply cannot probe -- a situation that will persist even beyond the commissioning of 100-m class telescopes. We have shown that low-mass (~1 $M_\odot$) T-Tauri and intermediate-mass (2-3 $M_\odot$) Herbig Ae stars share striking similarities in their polarized light properties at Hα, suggesting rotating accretion discs (Vink et al. 2002, 2003, 2005a, 2005b). Herbig Be stars (with masses of up to 10 $M_\odot$) are found exactly at the border where current theory becomes challenging, and they are the highest mass Young Stellar Objects (YSOs) that are visible in the optical part of the electromagnetic spectrum. In order to probe the circumstellar geometry of the most massive YSOs, we must use diagnostics at near-infrared (NIR) wavelengths, as more massive young stellar objects remain optically obscured throughout their entire pre-main sequence lives. There is currently no common-user infrared facility in operation that offers the desired combination of spectral resolution and sensitivity. SALT/RSS will become the first instrument to perform this new science on massive star formation.

6.4.1 Instrument Requirements

- Simultaneous optical-NIR longslit spectropolarimetry at R > 4000 out to 1.35 μm to sample Hα and NIR line diagnostics.
- Simultaneous optical-NIR MOS at R > 4000 out to 1.35 microns to sample Hα and Paβ (1.28 μm).
- Extension to 1.65 μm allows measurement of Paβ out to z=0.3, roughly the Sloan volume.

7 Supernova Explosion Physics

Our understanding of supernovae (SNe) has an impact on a wide variety of astronomical fields, from star formation, interstellar medium dynamics and chemical evolution of galaxies through cosmological models and the distance ladder. Yet there remain a number of basic unanswered questions in the field. For instance, it has been proposed that there are two distinct subclasses of SN Ia, distinguished by their different delay times between progenitor-star formation and SN explosion (Mannucci et al. 2006), which would have an obvious impact on the SN Ia distance ladder. One important aspect of SNe not yet well understood is their asymmetry, which may impact their observed brightness (in the case of SNe Ia) as well as the deposition of kinetic energy and enriched material into their environment. We have broad indications of SN asymmetry both from theory and from observation. High proper-motion pulsars from SNe, gamma-ray bursts and asymmetric remnants support the idea observationally for core-collapse SNe; the leading theories of SNe Ia progenitors imply breaking of symmetry (Wang & Wheeler 2008), as do jets and off-center ignition in explosion models.

Observational probes of SN asymmetries have been challenging: the most effective way of probing the asymmetries in SNe is with spectropolarimetry, and this has been pursued only recently with the advent of spectropolarimeters on 10m class telescopes. In SNe, polarization is thought to arise from electron scattering in the last few optical depths within the photosphere: a net continuum polarization of the integrated light results from an asymmetry of the photosphere, while polarization in the P-Cygni lines results from asymmetries in the overlying ejecta , which shadow asymmetric parts of the photosphere. By measuring the variation of line polarization with wavelength, we can observe asymmetries as a function of velocity (in SNe, this is equivalent to radius) so that line polarization gives us information

about chemical and density inhomogeneities within the ejecta, which can be compared with the results of explosion codes. Core–collapse supernovae show evidence of an underlying axisymmetric explosion mechanism, and also show significant deviations from that axisymmetry in individual cases. SNe Ia appear to be quite symmetric at their core, but show significant deviations from symmetry at early times, particularly in line profiles. Different lines show different polarization, indicating that the thermonuclear processing of the explosion is inhomogeneous.

SALT/RSS will be the first instrument capable of SNe spectropolarimetry in the NIR, bringing in a range of unobserved lines that are important for constraining explosion physics models. Especially interesting in SN Ia are the [Fe II] lines at 1.26 and 1.65 microns. Combining information from these lines with those of Si and Ca in the visible will trace elements produced in the full range of the thermonuclear explosion chain for the first time. Following each SN regularly throughout its light curve will show how this evolves as the envelope becomes optically thin. Doing it for a statistically useful number of SNe will then determine whether SNe can be divided into further subclasses based on structure.

7.1 Instrument Requirements

- Simultaneous optical-NIR longslit spectropolarimetry at R > 500 out to 1.65 μ. S/N ~ 1000 (0.1% polarization) is required.
- The maximum spectral coverage is required in one observation since these are time variable objects. These are bright objects (V = 13 – 16), so night sky is not an issue.
- Imaging polarimetry of the SN fields to remove foreground Galactic interstellar polarization.

8 Balancing the Baryon Budget: probing, star formation, gas accretion and feedback in z=1.5 galaxies

Galaxy evolution is driven by the process of gas accretion, feedback, and merging. There have been many studies of galaxy mergers in the last few years. Important theoretical work on accretion and

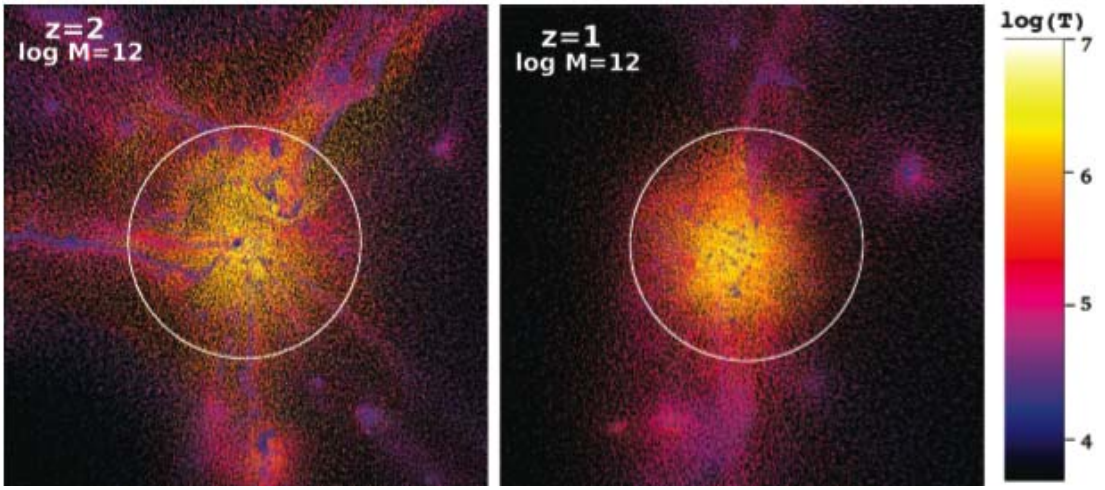

Figure 13. Simulation of gas temperatures in a Milky Way sized-halo at z=2 and z=1 from Keres et al. 2009. The box shown is 1 Mpc on a side. The circle is the virial radius. Note the coexistence of hot and cold gas.

feedback have resulted (**Figure 13**), but very few observations exist. The baryon-to-dark matter ratio measured in isolated galaxies is much lower than in galaxy clusters. Could the "missing" baryons be in hard to observe phases related to accretion and feedback (e.g., small clumps of cold gas, diffuse hot gas)?

In the next few years several large NIR photometric surveys will document the stellar content of galaxies from z=1-6. One such survey is the Spitzer Extragalactic Representative Volume Survey (SERVS). This is a 1400 hour Spitzer warm mission survey, which will obtain deep imaging at 3.6 an 4.5 um over 18 square degrees in 5 southern fields, overlapping the VISTA-VIDEO near infrared and Herschel-HERMES and SCUBA2-S2CLS far-infrared surveys. *NIR **spectroscopy** is a crucial to understand the nature of the gas in and around these galaxies.* We could conduct an RSS follow-up survey of approximately 100 galaxies at z=1.45 -- 1.65, selected to span a range of stellar mass, star formation rates (SFR), SFR/mass, and dust attenuation. These observations would utilize simultaneous visible and NIR multi-object spectroscopy, typically with 3-10 targets per pointing.

8.1 Probing star formation, gas accretion and feedback at z=1.5

At this redshift optical light (5500 - 7500 Å) traces the restframe UV. Features in this region include the interstellar medium absorption lines CIV, Fe II, Mn II, Mg II, Mg I, as shown in **Figure 14**. The near-IR probes optical nebular lines: J-band: H-beta, [O III], H-band: H-alpha, [NII], [SII], as shown in **Figure 15**.

8.1.1 Are the physical conditions in z=1.5 star-forming galaxies similar to those of local galaxies?

An approach to answering this question is to look for offsets in the [NII]/Hα vs. [OIII]/Hβ diagram (**Figure 16**). Do offsets correlate with SFR, SF surface density, mass, etc? Is there evidence for higher

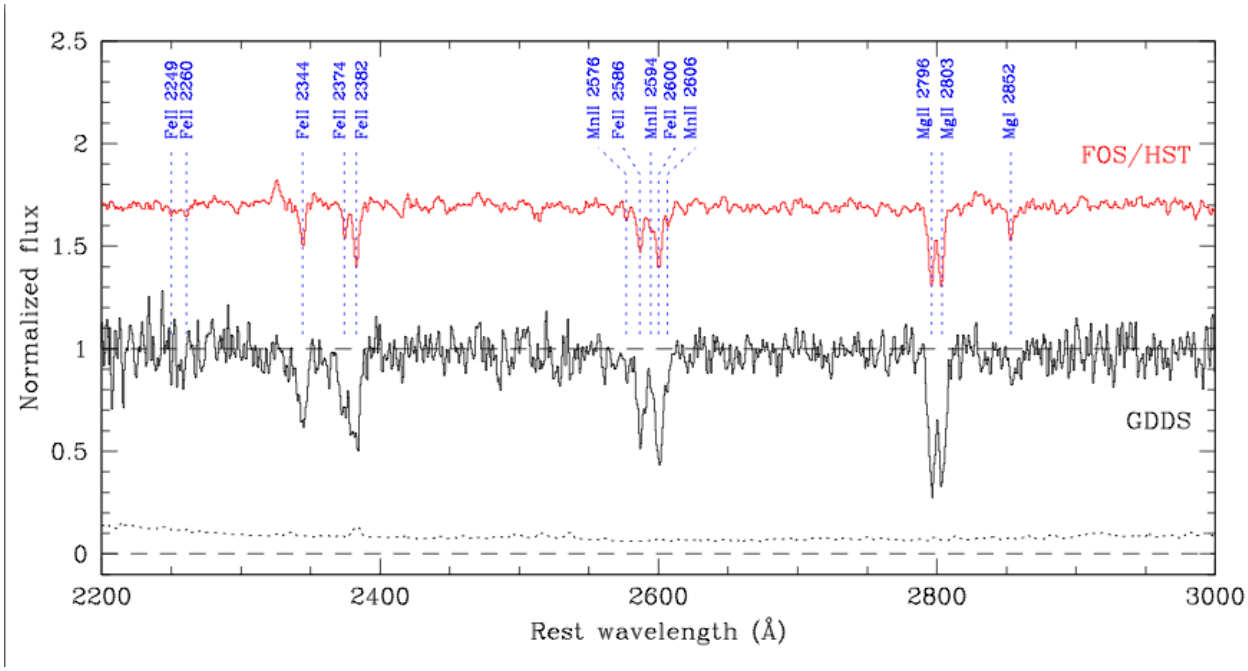

Figure 14. GDDS composite spectrum of 13 star forming galaxies at z=1.3 - 2 (Savaglio et al. 2004 - Gemini GMOS).

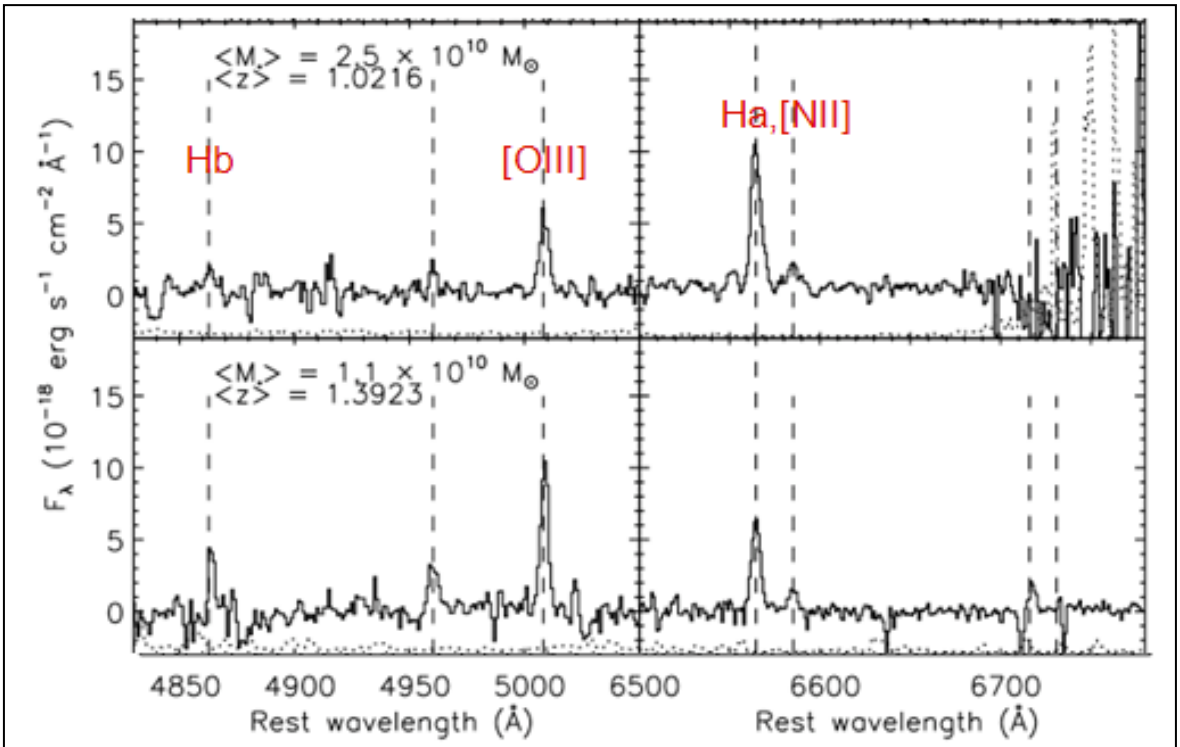

Figure 15. Composite restframe optical spectrum of 12 galaxies at z=1 - 1.5 (Liu et al. 2008 - Keck NIRSPEC).

densities or pressures?

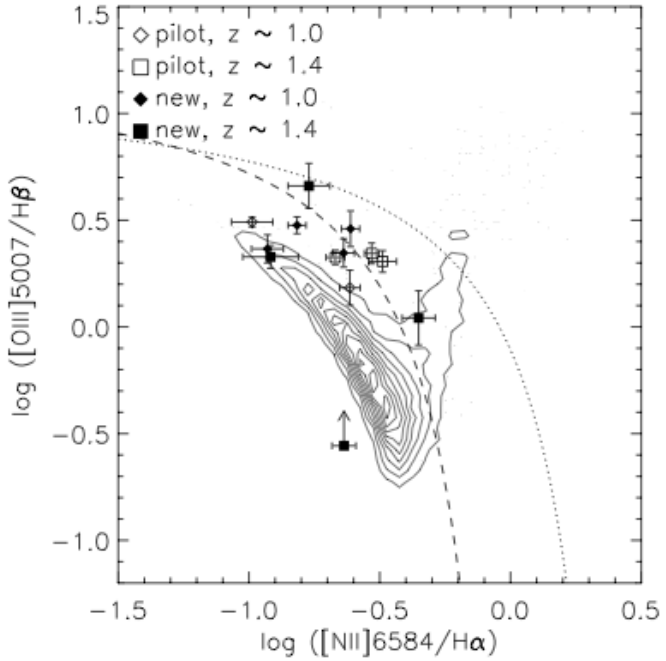

Figure 16. [NII]/Hα vs. [OIII]/Hβ diagram (Liu, Shapley, et al. 2008).

8.1.2 Does strong feedback drive gas outflows?

Look for evidence of galactic winds by measuring the relative velocity of the absorption and emission lines (emission lines trace gas in H II regions due to density squared dependence of the emission process). Does the outflow velocity depend on the ionization state of the gas? Compare CIV, Mg II, Mg I velocities. Does outflow velocity correlate with SFR, Mass, SFR/M, etc?

8.1.3 Are gas inflows required to account for the gas, stars and metals in the galaxies?

Following Erb et al. 2008, compare SFR/M and galaxy age (from SED

fitting) to simple models to infer the ratio of inflow to "gas processing" (SFR+outflow). Compare the gas fraction and metallicity to infer inflow and outflow rates relative to the SFR.

9 Phases of Galaxy Evolution

An important aspect of galaxy evolution is what happens to the galaxy and its central supermassive black hole during mergers. Some models of galaxy mergers are now predicting that an AGN phase is part of the process (Cox et al. 2008), possibly explaining the connection between the black hole mass and the galaxy mass (Gebhardt et al. 2000, Ferrarese & Merrit 2000). Many E+A galaxies, post-starburst objects, and host galaxies of luminous quasars show obvious signs of past interactions, supporting this unified idea.

9.1 E+A Galaxies

The star formation history of merging galaxies is a powerful diagnostic of galaxy evolution. Mergers construct large galaxies from smaller ones, and elliptical galaxies from spirals; in the process, they can form substantial fractions of the stellar populations of the newly merged system. Unfortunately, the complexities of merger-triggered star formation are not well understood (Lin et al. 2007). While a strong starburst event generally occurs at the onset of a merger, substantial tidal interactions, dynamical disturbance of the gas content, the possible triggering of AGN, and infall of tidally ejected gas all occur during the 10^9 years or more that mergers can take to complete.

Spatially-resolved spectroscopic studies of E+A galaxies, objects thought to be late stage galaxy mergers, have found both uniformly distributed and centrally concentrated post-starburst regions (Yagi & Goto 2006, Goto 2006, Goto et al. 2008a, Goto et al. 2008b), possibly suggesting different formation conditions. The centrally concentrated post-starbursts occur in galaxies both with and without optical spectral signatures of AGN. It is likely that gas falling to the center of the galaxy during a merger triggers

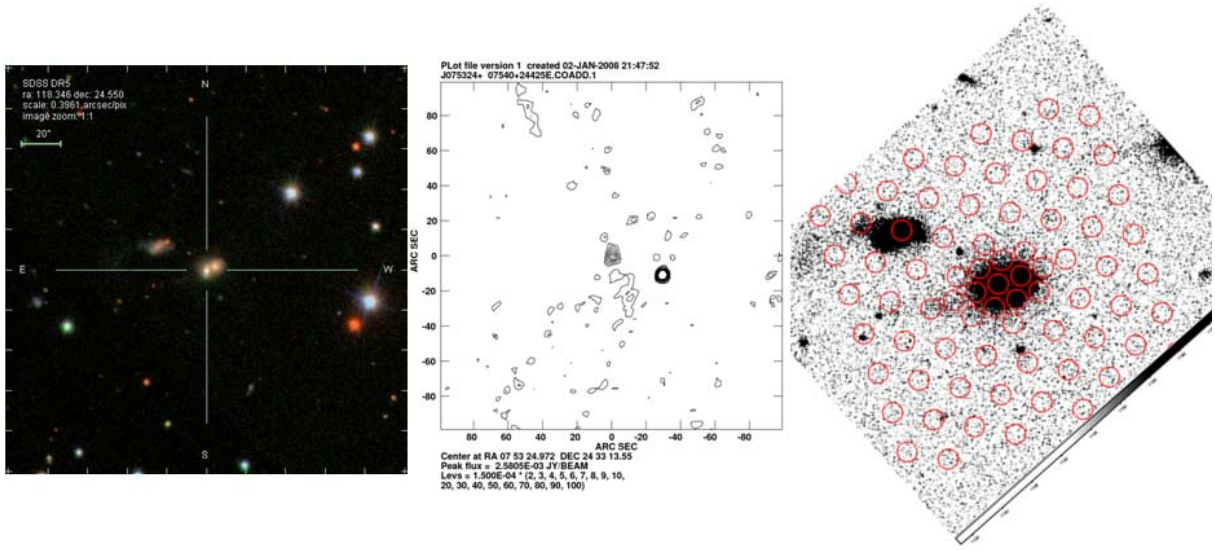

Figure 17. Observations of an E+A galaxy with a likely buried AGN (SDSS J075323.0+243300). Left: SDSS image. Center: radio map. Right: Integral field spectroscopy setup using SparsePak on WIYN.

both nuclear starbursts and AGN activity. If so, what about the centrally concentrated post-starbursts with no AGN signatures? Has the AGN turned off, or is it there at low luminosity or obscured by dust?

We are currently exploring the radio properties of E+A galaxies whose SDSS optical spectra indicate at most weak ongoing star formation (Goto et al. 2008b), and in many cases the galaxies appear to be quiescent passively evolving systems which had their last major burst of star formation several hundred Myr in the past. We have identified a sample of these with detectable radio fluxes in the NVSS and/or FIRST surveys, beginning with what we consider an archetype of the class, G515 (Liu et al. 2007). On the surface, the radio flux would indicate the presence of ongoing star formation, presumably buried in the central regions of the galaxy, since there is little or no optical evidence of current star formation. However, many of these objects show likely radio variability and/or extended radio lobes reminiscent of powerful radio galaxies (Hooper et al. 2007). While these are not luminous radio galaxies, the variability and extended morphologies strongly suggest the presence of low-luminosity AGN. Recent VLA observations of this sample of 14 objects will confirm or disprove the existence of buried AGN in these galaxies.

In parallel we are conducting an observing campaign using the SparsePak integral field unit to obtain spatially resolved spectroscopy on these galaxies (**Figure 17**). These spectra will result in spatially distributed stellar populations and NIR images using WHIRC on WIYN will allow the construction of extinction maps. With these data we should be able to tell the star formation histories in these galaxies,

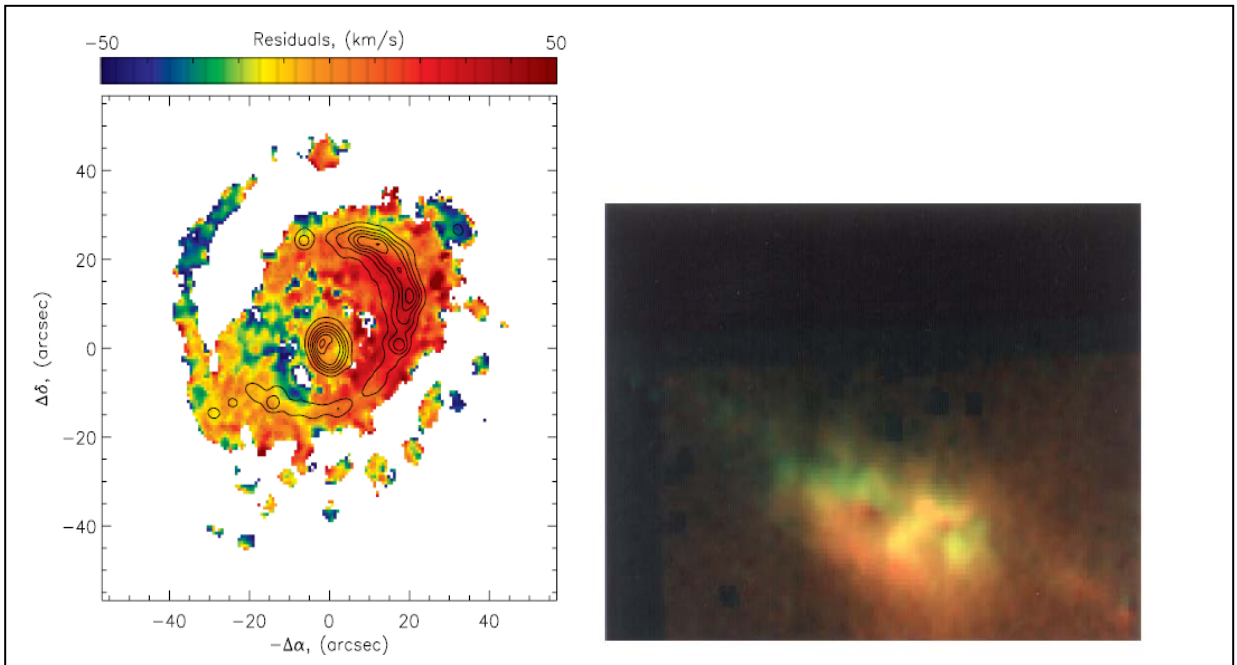

Figure 18. Fabry-Perot observations of galaxies. Left: Scanning FP at 40 km/s (Bizyaev et al, 2007, ApJ, 662, 304). Line-of-sight velocity residuals in Arp 10. A contour map of Ha emission is superimposed by thin black contours. Right: FP observations of M82 at resolution of 375 km/s (Greenhouse et al.,1997, ApJ, 476, 105). A composite image of the [Fe II] (red) and Brg (green) integrated line intensity. Yellow is a mixture of these components. The Brg data are from Satyapal et al. (1995). [Fe II]/H II line ratios can yield a relative age-dating technique for starburst clusters.

and infer the associated stellar mass assembly history in merged galaxies.

RSS will contribute to our understanding of these systems through simultaneous Fabry-Perot imaging to map out emission lines due to star formation in the visible arm (Hα, [O II]), and those due to shocks from supernova in the NIR arm ([Fe II], Paβ). Some examples are shown in **Figure 18**. We can also generate velocity maps of gas from which information about the geometries of past interactions can be inferred. Spectropolarimetry may reveal polarized spectra of hidden broad lines in the AGN.

9.2 Quasar Host Galaxies

Increasing evidence over the past decade, both observational and theoretical, has linked the growth of galaxies and their central supermassive black holes. We have an ongoing project in which we are studying luminous quasars ($M_V < -23$) and their host galaxies – objects where the galaxy is actively feeding the central black hole. We have developed a unique technique for observing the faint host galaxies in the presence of quasars that are as much as 3.5 mags brighter. The large fibers of SparsePak allow us to offset the quasar near the edge of one fiber and sample the host galaxy with two neighboring fibers. With slightly longer exposure times the SparsePak/Bench combination allows us to exploit the AΩ advantage and provides similar S/N at a higher spectral resolution, R, than previous Keck long-slit observations (110 km s^{-1} vs. 300 km s^{-1}). **Figure 19** shows the observational setups. With this technique we have directly measured the stellar velocity dispersion, σ_*, in the host galaxies of luminous quasars.

To date, the project has found that when a sample of 10 QSO hosts are compared to "normal" galaxies, the hosts of the radio-loud quasars occupy the upper extreme of the Fundamental Plane (**Figure 20**) and tend to be very massive galaxies with higher σ_*, larger radii, and lower surface brightnesses than quiescent elliptical galaxies (Wolf & Sheinis 2008). The radio-quiet QSO hosts have properties more

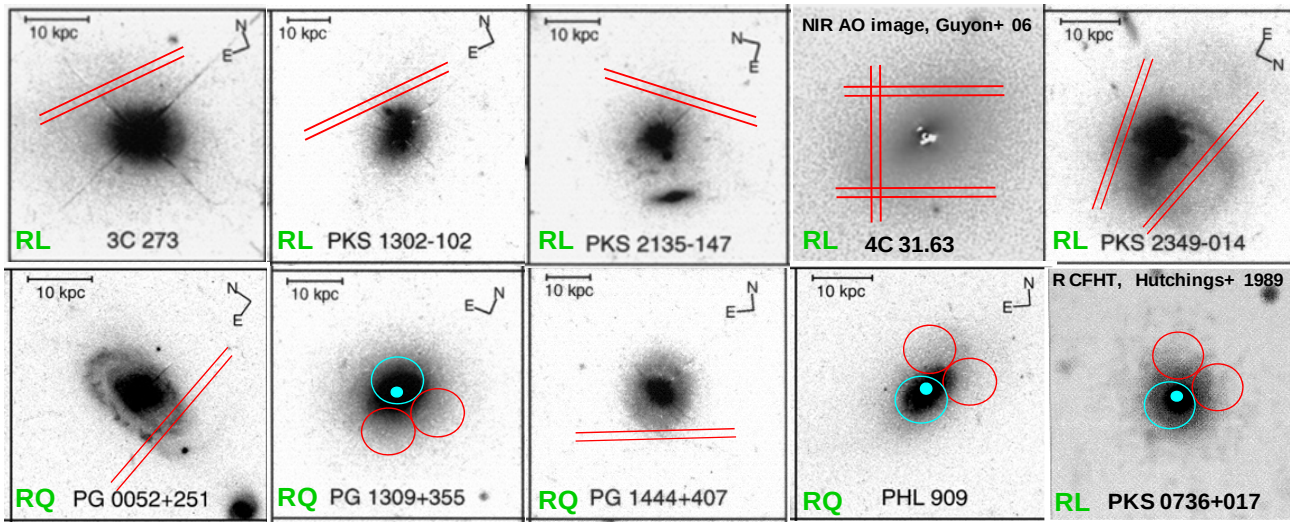

Figure 19. Observations of quasar host galaxies with long slits on the Keck Telescope and with the SparsePak optical fiber bundle on the WIYN Telescope. Each panel is 23 x 23 arcsec. Fiber circles are 5 arcsec in diameter, and the dots inside them mark the approximate locations of the quasars. For clarity, only 3 of SparsePak's 82 fibers are shown. RL denotes radio-loud quasars and RQ denotes radio-quiet. Our sample is drawn primarily from the 20 nearby luminous quasars of Bahcall et al. (1997), from which the underlying images are taken unless otherwise noted.

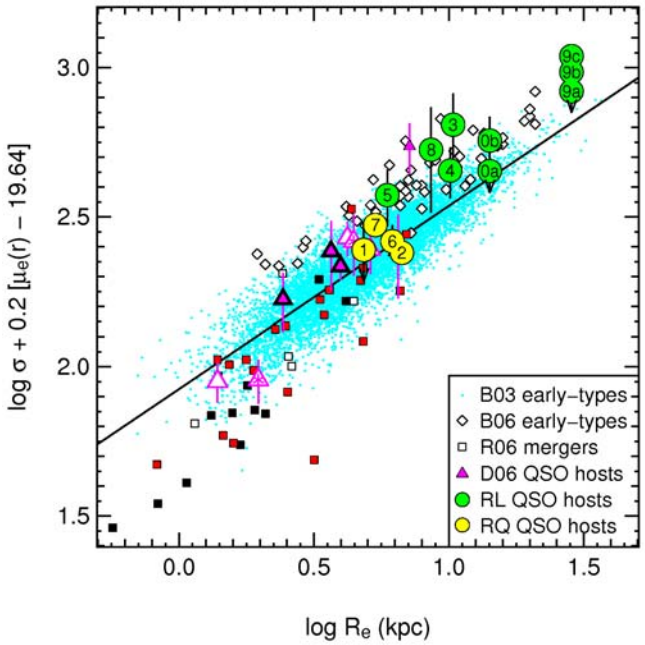

Figure 20. The Fundamental Plane of galaxies. Our quasar hosts are shown as large circles (yellow are radio-quiet, green are radio-loud). Comparison galaxies: small cyan points are early-type galaxies from SDSS (Bernardi et al. 2003), open diamonds are massive early-type galaxies (Bernardi et al. 2006), triangles are radio-quiet PG QSO hosts (Dasyra et al. 2007), and squares of all shades and colors are merger remnants (Rothberg & Joseph 2006). The solid line is the FP fit to early type galaxies from Bernardi et al. (2006).

similar to intermediate mass elliptical galaxies. We are now investigating the location of these objects on the M_{BH}-σ_* relation (Sheinis, et al., in prep). And finally, we are investigating the stellar populations in the host galaxies to look for signs of star formation during the quasar phase, or in a previous merger (Wold et al., in prep).

RSS on SALT will allow us to continue this work using the Ca IR triplet to measure host galaxy velocity dispersions, and will allow observations of lower surface brightness hosts than possible on the 3.5-m WIYN telescope. The NIR allows improvement of the host galaxy/quasar S/N because the quasar brightness is lower in the NIR than in the optical. The wide field of RSS will allow simultaneous observations of the environments by simultaneously observing companion galaxies with MOS spectroscopy. We can also study the polarization of these objects with spectropolarimetry.

Sheinis 2002 found large structures of [O III] gas surrounding some of these objects, by creating velocity maps along long slit observations. Fabry-Perot observations of these objects will be very powerful to

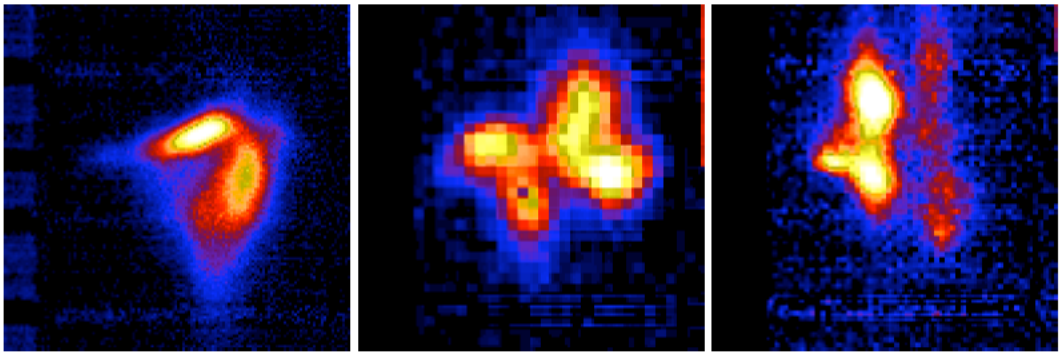

Figure 21. Two Dimensional extraction of the λ = 5007 Å line for 3C 249.1 for three different slit positions: (a) 3 seconds east; (b) 3.5 seconds north; and (c) 3 seconds west. Dispersion is in the vertical direction and encompasses ±787km s^{-1}. The slit runs along the horizontal dimension and encompasses ±29.8Kpc

look for interactions between the quasars, jets, and the surrounding ISM of the host galaxies. The combination of all of these observations will go far in explaining the histories of the formation and evolution of these objects.

10 Spectropolarimetry of Active Galactic Nuclei

Our entire picture of the universe is from light, mostly from total intensity. We generally discard the information in the Stokes parameters, U, Q, and V. But these parameters carry a wealth of information obtainable only by polarimetry, in particular spectropolarimetry. In Active Galactic Nuclei, there are two main polarization mechanisms - one intrinsic to synchrotron emission, the other the result of extinction. Extinction includes transmission through aligned dust grains that induces “dichroic” polarization. But of more interest is polarization by scattering - either by small dust grains or electrons. All these mechanisms are broad-band, and so require observations over a wide wavelength range -- UV through infrared.

The very significant role of dust in extragalactic studies is now appreciated. Surveys in the infrared and X-ray show that a large fraction of central AGN are obscured or partially obscured, and may be overwhelmed by host galaxy starlight. Spectropolarimetry over a wide wavelength range allows us to investigate the geometry of the central AGN and the obscuring and scattering material. This was first demonstrated for the Seyfert 2 AGN, NGC 1068, by Miller & Antonucci (1983), observations that lead to the “orientation Unified Scheme” in which the central AGN is surrounded by a dusty torus that obscures or partially obscures (reddens) the central AGN, but polar scatterers (thought to be usually dust grains) scatter light from the AGN continuum and broad line region (BLR) into the line-of-sight. The extended (100s--1000s pcs) narrow line region (NLR) is much less obscured. Spectropolarimetry allows us to distinguish this faint halo of scattered light, normally overwhelmed by light from the NLR and starlight. The axisymmetric torus picture was developed because the polarization position angle tended to be perpendicular (polar scattering) or parallel (disk scattering) to the radio jets, the latter defining the axis if the central engine. However, more generally, dust in polarized AGN is required to lie along the line-of-sight to the nucleus.

Such spectropolarimetric studies are important because these buried AGN contribute to the X-ray background, and because they provide a unique probe of the geometry of the AGN, the velocity field, and the properties of the scatterers. Understanding the relationship between extended properties (the host galaxy environment and NLR) and the central engine is necessary for understanding the tight relationship between black hole mass and host galaxy bulge properties (Gebhardt et al. 2000, Ferrarese & Merritt 2000, Tremaine et al. 2002). The dustiest, gas enshrouded AGN are an essential aspect of the hypothesis for the co-evolution of the black hole and spheroid -- representing the growth phase of the black hole, as the (Eddington ratio) radiation of the AGN blows away its birth-cocoon of dust and gas, revealing a luminous AGN. Both powerful infrared ultraluminous AGN and broad absorption line AGN (BAL QSOs) may be related to this process.

Some exciting clues from Spectropolarimetry are listed below.

1. The fraction of buried AGN. Some luminous AGN in the nearby Universe have been investigated by polarimetry, nearly always selected by the high equivalent width [OIII] at λ = 5007 Å emission line - a beacon for a buried AGN. Some examples are from the 2MASS NIR AGN survey (Smith et al. 2003), and also SDSS (Zakamska et al. 2005). However appears that not all [OIII] AGN show scattered-AGN light halos (Tran 2003). In addition, not all buried AGN have strong [OIII] emission (Wills & Hines 1997, Hines et al. 2001). These are two aspects that require spectropolarimetry of carefully-defined AGN samples. Percent (linear) polarizations range from >30% in the UV, to several percent in many "buried" AGN.

2. Probing the BLR by polarization across emission lines. Polarization changes across the broad emission lines has been shown to be a powerful probe of the kinematics in type 2 (strong NLR) AGN, but especially in type 1 (BLR) AGN, of the kinematics of circumnuclear material within the unresolved central parsec of AGN. Scatterers near the BLR view the kinematic structure from different angles, showing a disk-like BLR (Axon et al. 2008). Levels of polarization in type 1 AGN are of order ~ 1%.

3. Polarization due to scattering. High scattering polarization has been discovered in broad absorption line (BAL) QSOs. Their broad absorption troughs reveal outflows up to ~ 0.2c. Spectropolarimetry has confirmed that the outflows represent accretion disk winds. Only the very brightest 2-3 objects have been observed in this detail, and there is much more to be explored with this technique (Axon et al. 2008). Polarizations range from <1% to ~20% or more.

4. Continuum polarization in Seyfert 1s - non-buried AGN. Unpolarized Fe II and other emission line blends completely dominate Seyfert 1s in the region of the Balmer continuum. But often there is low level continuum-only polarization (p<~ 1%), thought to arise from electron scattering interior to the BLR, and it's been discovered that the polarized flux yields a Balmer edge in absorption. Thus, polarized light is used to de-contaminate the spectrum and investigate the Balmer edge spectral feature expected but never seen in accretion disk emission (Kishimoto et al. 2005). Because of the low-level polarization, and shallow Balmer edge depth, observations are at present difficult. But such observations are important because there are very few ways to investigate this continuum, which is energetically dominant in AGN.

5. Reverberation mapping of polarized AGN. Goosmann et al. (2008) describe a polarization/radiative transfer code to predict the effect of continuum variations on the light-travel time delays of photons transmitted and scattered within a simple filled cone (as in simple Unified Schemes, above). While this technique has not revealed clear results as yet, it is potentially feasible and powerful.

6. Broad Absorption Line (BAL) QSOs. Polarization is much more common in luminous BAL QSOs than their non-BAL counterparts, and some BAL QSOs show evidence for several light paths: the relativistic absorbing outflows can be seen in polarized and/or unpolarized light in different atomic species and with different velocity profiles demonstrate complex geometry (eg, Glenn et al. 1994, Hines & Wills 1995, Cohen et al. 1995, Ogle et al. 1999).

Huge contributions can be made by RSS on SALT, especially with the NIR extension. Possible observations are described below.

(i) All AGN spectropolarimetry suffers from limited polarized photon statistics. The high efficiency of the RSS (UV through NIR) and large telescope aperture will allow many AGN to r~17.5 to be studied with medium resolution, and fainter objects to 18.5 mag, with R~4000 resolutions, working between skylines. Note that working with polarization levels of 1% to 10% is approximately equivalent to observing objects 5 to 2.5 magnitudes fainter than their total magnitudes.

(ii) Ability to compare continuum polarization over a huge wavelength range. (a) The distinctive wavelength dependence of interstellar polarization can be largely corrected. (b) The wavelength independence of electron scattering, and the wavelength dependent dust scattering can, in principle, be distinguished. (c) Using the UV-optical and NIR coverage, polarization across several line species can be compared. This is true for emission lines (item 2) and absorption lines (item 3).

(iii) The scheduling on SALT should allow frequent (time scales of ~days) monitoring for variable flux density and polarized flux density in selected objects.

Samples for the above observations can be made from many surveys available, such as SDSS, 2MASS, FIRST, partially-obscured AGN found as UV-optical identification of Chandra sources, etc. The SDSS provides a wealth of type 1 and type 2 AGN/QSOs, and BAL QSOs. The FIRST survey provides clues to jet directions that can sometimes be directly related to polarization position angles. Detailed spectropolarimetry across BALs and emission lines would require S/N of a few percent in polarized flux, but for statistical or continuum samples the data could be binned in wavelength to achieve this level.

11 Summary of Science Requirements

The main science programs planned by the University of Wisconsin and their instrument requirements are summarized in **Table 6**.

Table 6. Instrument requirements of main science drivers from UW.

Project	Description	z	RSS Mode	R	Long λ (μm)	Sensitivity Limit (erg s^{-1} cm^{-2})	Simultanous Observations
Ultra-high Redshift Universe: Discovering First Light	Discover when and how rapidly the first galaxies formed. When is reionization complete?	z <= 10	Fabry-Perot	2500	1.35	1.00E-18 1 M_{sun} yr^{-1}	visible FP tuned to redshifted [OII]3727 if NIR line is Hα
		z = 12-13	Fabry-Perot	2500	1.65	few M_{sun} yr^{-1}	

Project	Description	z	RSS Mode	R	Long λ (μm)	Sensitivity Limit (erg s^{-1} cm^{-2})	Simultanous Observations
Star-Formation in the "Desert:" When Galaxies Were Young	Map star-formation rate and dynamical masses using [OII]3727 in the 1.4<z<2.6 regime when most of the mass-assembly for massive galaxies is believed to have taken place.	1.4 < z < 2.6	MOS	> 4000	1.35	≥ 1 M_{sun} yr^{-1}	visible MOS to cull interlopers and acquire multiple lines for metallicity estimates and ISM diagnostics
	well-beyond peak in comoving SFR and AGN activity	z < 3.4	MOS	> 4000	1.65		
Baryon Processing in a Mature Universe	Precision mapping of down-turn in co-moving SFR and chemical enrichment from 0<z<1 as function of dynamical mass using Ha and strong-line nebular diagnostics ([NII]/ Hα, [OIII]/ Hβ)	z < 1	MOS	> 4000	1.35		Simultaneous optical-NIR MOS at R>4000 out to 1.35 μm; split[OII]3727 doublet and cull interlopers; acquire multiple lines for metallicity estimates and ISM diagnostics.
	kinematics of narrow-lined (σ<70 km/s) systems at the low-mass end		MOS	7000	1.35		
Baryon Processing in a Mature Universe		z < 1.5	MOS		1.65		

Project	Description	z	RSS Mode	R	Long λ (μm)	Sensitivity Limit (erg s^{-1} cm^{-2})	Simultanous Observations
Massive Star-formation at z = 0	Constrain theories of massive star-formation that link production of elements and luminosity, to the energetics of feedback mechanisms and chemical enrichment which drive the evolution of baryons in galactic systems. Hα/Paβ flux ratios in obscured, star-forming regions and linear spectropolarimetry of circumstellar regions in obscured sources are the primary measurements.	z = 0	longslit spectro-polari-metery	> 4000	1.35		Simultaneous optical-NIR MOS at R>4000 out to 1.35 μm to sample Hα and Paβ (1.28 μm)
	Paβ out to z=0.3, roughly the Sloan volume	z < 0.3			1.65		
Supernovae Explosion Physics	Measuring the variation of line polarization with wavelength to observe asymmetries as a function of velocity so that line polarization gives information about chemical and density inhomogeneities within the ejecta, which can then	z = 0	longslit spectro-polari-metery	> 500	1.65	S/N = 1000 (0.1% polarization)	Maximum spectral coverage is required in one observation since these are time variable objects. Simultaneous VIS spectro-polarimetry to

Project	Description	z	RSS Mode	R	Long λ (μm)	Sensitivity Limit (erg s^{-1} cm^{-2})	Simultanous Observations
	be compared with the results of explosion codes						get additional time-variable lines. Imaging polarimetry of the SN fields to remove foreground Galactic interstellar polarization.

11.1 Science – Engineering Trade Matrix

The table below summarizes instrument engineering decisions that would affect capabilities and thus the science programs that could be conducted. Time percentages for different long wavelength cutoffs are % of hours between 18° astronomical twilight throughout a year, based on historical SALT temperature data. (See the RSS-NIR Thermal Stray Light Analysis, document # SALT-3501AA0002, for derivation of these numbers.)

Table 7. Science – Engineering Trade Matrix.

Engineering Decision	Option	Capability Change / Complexity Implications	Science Affected	Engineering Impact	Cost Estimate
Pre-dewar cooling	none	λ_{cutoff} limit at 1.35 μm; Compromises probability of overall instrument success	Lose: Galaxy diagnostics at z>1; Thermal shocks from supernova remnants ([Fe II], 1.644 μm) and recombination processes in young HII regions (Br 12-4 [1.641 μm], Br 13-4 [1.611 μm], and Br 14-4 [1.588 μm]); Lyα at z>10	Straightforward: This would reduce requirements in the design.	Reduce baseline budget by $280k
	cool to -40 °C	Components in pre-dewar will not thermally limit operation	Allows observations out to λ ~ 1.55-1.67 μm; Lyα to z~13	Manageable: This is the current baseline requirement. Many components operational to this temperature.	None – in the baseline budget.
	cool below -40 °C	Minimal performance increase, unless entire instrument is cooled and longer wavelength detector used	None, given our 1.7 μm detector cutoff wavelength	Difficult: Electronics and motors will be difficult to find, it is a rare exception that an off-the-shelf item is rated this low. Larger load on the chilling system.	Increase baseline by $75-125k (materials and labor)

Engineering Decision	Option	Capability Change / Complexity Implications	Science Affected	Engineering Impact	Cost Estimate
Slit cooling (assuming gold slits)	none	λ_{cutoff} for R=7000 (4000): 1.65 μm 7% (29%) of time, 1.6 μm 47% (74%) of time, 1.55 μm 86% (100%) of time	Compromises many diagnostic lines in λ = 1.6-1.67 μm region	None	None
	cool to dT_{slit} = 30 ^{o}C below T_{amb}	λ_{cutoff} for R=7000 (4000): 1.7 μm 41% (69%) of time, 1.65 μm 90% (99%) of time, 1.6 μm 100% (100%) of time	More likely to be able to observe Fe II 1.644 μm line and Br lines at λ > 1.6 μm	Challenging: This has been assessed and viable options have been developed. This will require some bench testing to verify and test a design scheme.	Increase baseline by $150-200k
	cool more than dT_{slit} = -30 ^{o}C	Only incremental long λ performance increase, unless collimator is also cooled	Not much gained	Difficult: Removing enough energy and mitigating condensation become very difficult beyond 30 °C below ambient.	Increase baseline by $175-250k
Collimator cooling	none	Does not affect performance unless the slit is cooled to dT_{slit} > 30 ^{o}C below $T_{ambient}$	Not necessary for main science cases	None	None

Engineering Decision	Option	Capability Change / Complexity Implications	Science Affected	Engineering Impact	Cost Estimate
	cool	Could go to longer wavelength detector; More stringent specs on long wavelength cutoff filters; Compromises probability of overall instrument success	Observe higher redshift objects, Pa-α line, better data on asteroids & KBOs at longer wavelengths	Challenging with risks: The collimator is significantly spaced limited by, one, original design that compensates alignment over a larger temperature range and, two, the spaceframe. May require remounting the optics to take advantage of radial space for cooling. Exposes optics and coatings to significant risk.	Increase baseline by $275-375k
Number of gratings	increase from 5	Would decrease gaps in contiguous spectral coverage between gratings at a given R for R>4000; Could extend to R>7000 or 800<R<4000 Would decrease number of available FP filters	Improve chances of observing particular redshifted lines at a specific R; Would increase contiguous spectral coverage for stellar populations in galaxies; Decreases spectral windows for FP observations (filters)	None to challenging: If the number of filters are reduced to provide space, there is no impact. If not, this is very challenging if not difficult. RSS-NIR is pushing the SALT envelope now.	~None: if gratings are swapped for filters. Adding a grating: ~$25k (w/ redesign, holder, grating…)
Exchangeable gratings	while pre-dewar is cold	Increases timing flexibility of observations at R > 7000 or 800 > R > 4000 to days rather than months	Quicker observations of bright objects at intermediate or very high R	Challenging: Requires new scheme and design to isolate and remove grating cassette. Can be done, but significant engineering time required.	Increase baseline by: $75-125k

Engineering Decision	Option	Capability Change / Complexity Implications	Science Affected	Engineering Impact	Cost Estimate
	only when pre-dewar is warm	Forces above observations to campaign mode	Have to observe R>7000 in campaign mode	None: in baseline plan	None
Number of FP filters	increase from 12	Would allow FP observations in more atmospheric windows; Would mean fewer gratings in pre-dewar	More flexible observations of redshifted objects: high z Lyα emitter search	Challenging: RSS-NIR is pushing the SALT envelope now. No space available.	Increase baseline by: ~$25k per filter
Number of exchangeable FP filters	increase from 3	Would decrease required frequency of filter exchanges	More flexible observations of redshifted objects; Otherwise delayed by ~days-weeks for filter exchanges	Manageable: Can be done, up to 6. Impacts: 1) heavier cassette for handler. 2) Potentially needless thermal cycles on filters that do not need to be removed	Negligible: Redesign of preliminary design, ~$5k
Gold coating long slits	none	λ_{cutoff} limit at 1.5 μm	Lose: Galaxy diagnostics at z~1-2; Thermal shocks from supernova remnants ([Fe II], 1.644 μm) and recombination processes in young HII regions (Br 12-4 [1.641 μm], Br 13-4 [1.611 μm], and Br 14-4 [1.588 μm]); Lyα at z>11	Straightforward: Simply need to coat slits.	$150-300 slit
Gold coating MOS masks	none	λ_{cutoff} limit at 1.5 μm; Decreases complexity, time, cost of making masks	same as above	Manageable: Working on processes to gold coat. Will add lead time to order and receive mask blanks at facility.	Operational increase: $150-300/mask

Engineering Decision	Option	Capability Change / Complexity Implications	Science Affected	Engineering Impact	Cost Estimate
ADC	Remove for NIR observations	Would improve NIR performance	Problem for simultaneous UV-NIR observations	None	SALT Facility
Dichroic split λ		Determines whether Ca IR triplet is on VIS or NIR arm	None Nominally at 0.9 μm		
Exchangable Dichroic	Manual process during the day	Would allow more than one split wavelength, fold mirror for only VIS observations, straight through for only NIR observations	Spectropolarimetry may have issues with a dichroic beamsplitter – would be forced into campaign mode with manual change	Challenging: Requires a redesign of the dichroic and Vis & NIR doublets mounts to streamline access and alignment. Very tight and difficult working conditions.	Increase baseline by: ~$30k + cost of additional optics
	Remote process during observing	Would allow more than one split wavelength, fold mirror for only VIS observations, straight through for only NIR observations	More flexible timing for spectropolarimetric observations if dichroic is a problem	Difficult: The tight space may make this impossible. Significant engineering time required for concept, preliminary, detail design. Additional fabrication and testing required.	Increase baseline by: ~$175-250k

11.2 System Overview

Very high efficiency VPH transmission gratings are available. This allows a compact, efficient, all transmissive system with a simpler camera. Visible VPH gratings are installed and commissioned in the RSS-visible beam. Because the gratings will be used at angles of up to 100 degrees (between collimator and camera), the spectrometer can produce a higher dispersion than a conventional reflection-grating spectrometer from a moderate beam diameter. This allows the spectrometer to be as compact as possible.

The scientific and technical requirements of RSS-NIR have led to the following baseline system design.

1. Instrument modes
    a. Imaging
    b. Spectroscopy
        i. Long slit
        ii. MOS
    c. Fabry-Perot narrow band imaging
    d. Polarimetry
        i. This mode can be added to any other modes
2. A fixed dichroic beamsplitter separates the visible and NIR arms of RSS. The nominal wavelength at which the split happens is 0.9 μm.
3. RSS-NIR is laid out in sections operating at 3 different temperatures.
    a. Ambient temperature components include:
        i. Slit plane (slit cooling will be engineered as an upgrade)
        ii. Waveplates for polarimetry
        iii. Collimator
        iv. Dichroic beamsplitter
        v. Separate final collimator doublet for each arm to optimize image quality
    b. Pre-dewar operating at -40 ^{o}C encloses:
        i. NIR collimator doublet serves as the window to the pre-dewar. The air space between the doublet elements and on the outside of the first element will be purged with dry air to prevent condensation.
        ii. Fold mirror
        iii. 5 remotely deployable spectroscopic gratings:
            1. 4 VPHGs providing R ~ 4000-7000 (1" slit)
            2. 1 conventional grating or grism providing R~800
        iv. 1 remotely deployable Fabry-Perot etalon (R~2500)
        v. 12 remotely deployable Fabry-Perot order blocking filters
        vi. 1 remotely deployable polarizing beamsplitter for polarimetry
        vii. Camera optics – first 5 of 7 at pre-dewar temperature
    c. Cryogenic vacuum dewar operating at 120 K. Completely contained inside the pre-dewar. Cooled with a closed cycle cooling system. Dewar contains:
        i. Last 2 camera optics
        ii. Camera lens #6, IFPL51Y, is the window from the pre-dewar into the dewar
        iii. 5 position filter wheel: open, blocked, 3 long wavelength cutoff filters
        iv. Detector array: 2048x2048 HAWAII2-RG, 1.7 μm wavelength cutoff
        v. SIDECAR ASIC electronics
        vi. Temperature control system

4. Camera and gratings are each remotely articulated to set spectral resolution and central wavelength. Grating angles up to 50 degrees can be accommodated. Maximum resolution is 7000 with 1" slit, 14000 with 0.5" slit (minimum slit width at Nyquist sampling).
5. Camera focus is remotely controlled using a group of lenses in the pre-dewar, outside the cryogenic dewar. Focus mechanism is similar to that designed for the visible beam.
6. Camera optics will be held within metal cells by an elastomer, similar to the visible beam.
7. Fold mirror is actuated to allow nodding along the slit by 10's of arcsec during long spectroscopic exposures. A second tip/tilt stage on the fold mirror allows open loop flexure compensation.
8. Any of the 12 Fabry-Perot filters can be exchanged during the day while keeping the pre-dewar cold via an air lock system that allows the removal and replacement of a 3 filter cassette. This also allows guest or campaign filters to be inserted during normal daytime operation.
9. Custom multi-object slit masks are laser-cut with a system designed for the RSS visible instrument.
10. Slit masks will have a gold low emissivity coating, allowing sky-limited spectroscopy out to 1.55 – 1.67 μm, depending on the ambient temperature and the spectral resolution of the observations.
11. No slit cooling will be provided initially. A feasibility study has been done and viable solutions identified. This may be added as a later upgrade to allow sky-limited spectroscopy to be possible during more of the year and to extend out to 1.7 μm.
12. The NIR camera and doublet will have a small amount of passive optical compensation for focus with temperature as these optics will be held essentially isothermally within the dewar and pre-dewar.
13. Three cryogenic IR blocking filters will reside in the dewar to allow for a selectable maximum long wavelength spectral cutoff for sky-limited observations. The allowable cutoff wavelength will be based on the ambient temperature and spectral resolution of the observations.
14. Assembly and integration will occur offsite in at the SAAO facilities in Cape Town. The visible instrument will be shipped fully assembled to Cape Town for this procedure.

12 References

Axon, D.J., Robinson, A., Young, S., Smith, J.E., & Hough, J.H.\ 2008, Memorie della Societa Astronomica Italiana, 79, 1213

Becker, G.D., Rauch, M., & Sargent, W.L.W., 2008, arXiv: 0812.2856

Beletic, et al., 2008, Proc. SPIE, 7021, 70210H

Bernardi, M., et al. 2003, AJ, 125, 1817

Bernardi, M., et al. 2006, AJ, 131, 2018

Bershady, et al., 2004, astro-ph/0403478

Clavel, J., Wamsteker, W., & Glass, I. M. 1989, ApJ, 337, 236

Cohen, M.H., Ogle, P.M., Tran, H.D., Vermeulen, R.C., Miller, J.S., Goodrich, R.W., & Martel, A.R., 1995, ApJ, 448, L77

Cox, T.J., Dutta, S.N., Hopkins, P.F., & Hernquist, L., 2008, ASPC, 399, 284

Dasyra, K.M., Tacconi, L.J., Davies, R.I., Genzel, R., Lutz, D., Peterson, B.M., Veilleux, S., Baker, A.J., Schweitzer, M., Sturm, E., 2007, ApJ, 657, 102

Dasyra, K.M., Ho, L.C., Armus, L., Ogle, P., Helou, G., Peterson, B.M., Lutz, D., Netzer, H., & Sturm, E. 2008, ApJ, 674, L9

de Grijs, et al., 2004, MNRAS, 352, 263

Elmegreen, D.M., Elmegreen, B.G., Rubin, D.S., & Schaffer, M.A., 2005, ApJ, 631, 85

Ferrarese, L., & Merritt, D., 2000, ApJ, 539, L9

Gallagher, J.S., et al., 2008, A&A, 486, 165

Gaskell, M. 2008, RevMexAA, 32, 1

Gebhardt, K., et al., 2000, ApJ, 539, L13

Glenn, J., Schmidt, G.D., & Foltz, C.B.,1994, ApJ, 434, L47

Glickman, E., Helfand, D. J., & White, R. L. 2006, ApJ, 640, 579

Goosmann, R.W., Gaskell, C.M., & Shoji, M., 2008, SF2A-2008, 231

Goto, T., 2006, MNRAS, 369, 1765

Goto, T., et al., 2008a, MNRAS, 386, 1355

Goto, T., et al., 2008b, aph-0809.089

Hines, D.C., & Wills, B.J., 1995, ApJ, 448, L69

Hines, D.C., Schmidt, G.D., Gordon, K.D., Smith, P.S., Wills, B.J., Allen, R.G., & Sitko, M.L., 2001, ApJ, 563, 512

Hooper, E.J., Liu, C., van Gorkom, J., & O'Neil, K., 2007, BAAS, 39, 907

Kishimoto, M., Antonucci, R., Boisson, C., & Blaes, O., 2005, Astronomical Polarimetry: Current Status and Future Directions, 343, 435

Lancon, et al., 2007, A&A, 468, 205

Laor, A., 2007, in The Central Engine of Active Galactic Nuclei, ASP Conf. Ser. 373, 384

Lin, L., et al., 2007, ApJ, 660, L51

Liu, C., Hooper, E., O'Neil, K., Thompson, D., Wolf, M., & Lisker, T., 2007, ApJ, 658, 249

Mannucci, F., Della Valle, M., & Panagia, N. 2006, MNRAS, 370, 773

Miller, J.S., & Antonucci, R.R.J, 1983, ApJ, 271, L7

Nenkova, M., Sirocky, M. M., Nikutta, R., Ivezic, Z., & Elitzur, M. 2008, ApJ, 685, 160

Nestor, D.B., Turnshek, D.A., Rao, S.M., & Quider, A.M., 2007, ApJ, 658, 185

Ogle, P.M., Cohen, M.H., Miller, J.S., Tran, H.D., Goodrich, R.W., & Martel, A.R., 1999, ApJS, 125, 1

Portilla, J. G., Rodriguez-Ardila, A., & Tejeiro, J. M. 2008, RevMexAA, 32, 80

Ramos Almeida, C., Perez Garcia, A. M., & Acosta-Pulido, J. A. 2009, ApJ, 694, 1379

Rothberg, B., & Joseph, R.D. 2006, AJ, 131, 185

Ryan-Weber, E.V., Pettini, M., & Madau, P., 2006, MNRAS, 371, L78

Sheinis, 2002, PhD dissertation, University of California, -Santa Cruz

Smail, I., Ivison, R.J., & Blain, A.W., 1997, ApJL, 490, L5

Smith, P.S., Schmidt, G.D., Hines, D.C., Foltz, C.B., 2003, ApJ, 593, 676

Steidel, C.C., & Sargent, W.L.W., 1992, ApJS, 80, 1

Suganuma, M., et al. 2006, ApJ, 639, 46

Tran, H.D., 2003, ApJ, 583, 632

Tremaine, S., et al., 2002, ApJ, 574, 740

Wang, L., & Wheeler, J. C. 2008, ARA&A, 46, 433

Wills, B.J., & Hines, D.C., 1997, Mass Ejection from Active Galactic Nuclei, 128, 99

Wolf, M.J., 2005, PhD Dissertation, University of Texas at Austin

Wolf, M.J., & Sheinis, A.I., 2008, AJ, 136, 1587

Yagi, M., Goto, T., 2006, AJ, 131, 2050

Yang, Y., Tremonti, C.A, Zabludoff, A.I., & Zaritsky, D., 2006, ApJ, 646, L33

Zakamska, N.L., et al., 2005, AJ, 129, 1212